DRUG DELIVERY
2024, VOL. 31, NO. 1, 2392755
https://doi.org/10.1080/10717544.2024.2392755

Taylor & Francis
Taylor & Francis Group

RESEARCH ARTICLE

Development of a drug delivering round window niche implant for cochlear pharmacotherapy

Chunjiang Wei[a,b], Ziwen Gao[a,b,c], Martina Knabel[a], Martin Ulbricht[d], Stefan Senekowitsch[d], Peter Erfurt[a], Norman Maggi[f], Bastian Zwick[g], Thomas Eickner[h], Farnaz Matin-Mann[a], Anne Seidlitz[d,e], Thomas Lenarz[a,b] and Verena Scheper[a,b]

[a]Department of Otolaryngology, Hannover Medical School, Hannover, Germany; [b]Cluster of Excellence "Hearing4all", German Research Foundation (DFG, "Deutsche Forschungsgemeinschaft"), Hannover Medical School, Lower Saxony, Germany; [c]ENT Institute and Department of Otorhinolaryngology, Eye & ENT Hospital, Fudan University, Shanghai, China; [d]Center of Drug Absorption and Transport, Department of Biopharmacy and Pharmaceutical Technology, Institute of Pharmacy, University of Greifswald, Greifswald, Germany; [e]Institute of Pharmaceutics and Biopharmaceutics, University of Duesseldorf, Duesseldorf, Germany; [f]Carl Zeiss GOM Metrology, Braunschweig, Germany; [g]Carl Zeiss Industrielle Messtechnik GmbH, ZEISS Group, Essingen, Germany; [h]Institute for Biomedical Engineering, University Medical Center Rostock, University of Rostock, Rostock, Germany

ABSTRACT

Background: There exists an unfulfilled requirement for effective cochlear pharmacotherapy. Controlled local drug delivery could lead to effective bioavailability. The round window niche (RWN), a cavity in the middle ear, is connected to the cochlea via a membrane through which drug can diffuse. We are developing individualized drug-eluting RWN implants (RNIs). To test their effectiveness in guinea pigs, a commonly used model in cochlear pharmacology studies, it is first necessary to develop guinea pig RNIs (GP-RNI).

Methods: Since guinea pigs do not have a RWN such as it is present in humans and to reduce the variables in *in vivo* studies, a one-size-fits-all GP-RNI model was designed using 12 data sets of Dunkin-Hartley guinea pigs. The model was 3D-printed using silicone. The accuracy and precision of printing, distribution of the sample ingredient dexamethasone (DEX), biocompatibility, bio-efficacy, implantability and drug release were tested *in vitro*. The GP-RNI efficacy was validated in cochlear implant-traumatized guinea pigs *in vivo*.

Results: The 3D-printed GP-RNI was precise, accurate and fitted in all tested guinea pig RWNs. DEX was homogeneously included in the silicone. The GP-RNI containing 1% DEX was biocompatible, bio-effective and showed a two-phase and sustained DEX release *in vitro*, while it reduced fibrous tissue growth around the cochlear implant *in vivo*.

Conclusions: We developed a GP-RNI that can be used for precise inner ear drug delivery in guinea pigs, providing a reliable platform for testing the RNI's safety and efficacy, with potential implications for future clinical translation.

ARTICLE HISTORY
Received 18 January 2024
Revised 8 August 2024
Accepted 11 August 2024

KEYWORDS
Local inner ear therapy; drug delivery; 3D printing; round window niche implant; Guinea pig

1. Introduction

Inner ear disorders such as hearing loss, tinnitus and vertigo, have significant impact on the well-being of people worldwide. These conditions result in severe economic losses and the World Health Organization (WHO) estimates that unaddressed hearing loss poses an annual global cost of 980 billion dollars (World Health Organization., 2014). Therefore, finding effective therapeutic strategies for the inner ear is essential for the benefit of patients and the global economy.

Pharmacotherapy plays a central role in treating various inner ear disorders, including autoimmune diseases, cisplatin- or noise-induced hearing loss, and Meniere's disease. Extensive research has demonstrated the efficacy of numerous drugs in preclinical settings. Antioxidants such as N-acetylcysteine (Bielefeld et al., 2007; Rushworth & Megson, 2014), sodium thiosulfate (Choe et al., 2004; Bijarnia et al., 2015) and amifostine (Wang et al., 2019) have been shown to be beneficial in protecting against or treating hearing loss of various etiologies. In addition, many studies have indicated the beneficial effects of exogenous neurotrophic factors on the protection and regeneration of the nervous system. Prominent examples include NGF (Nerve growth factor) (Schindler et al., 1995; Shah et al., 1995), BDNF (Brain-derived neurotrophic factor) (Staecker et al., 1996; 1998; Gillespie et al., 2003), NT-3(Neurotrophin-3) (Ernfors et al., 1996; Staecker et al., 1996) and GDNF (Glial cell line-derived

CONTACT Verena Scheper Scheper.Verena@mh-hannover.de Department of Otolaryngology, Hannover Medical School, Stadtfelddamm 34, 30625 Hannover, Germany

neurotrophic factor) (Ylikoski et al., 1998; Yagi et al., 2000; Kanzaki et al., 2002). Among the diverse therapeutic options, glucocorticoids emerge as particularly noteworthy due to their widespread clinical use, which is primarily due to their potent anti-inflammatory and immunosuppressive properties. Since the 1950s and 1960s, glucocorticoid therapy has been used for autoimmune ear diseases, yielding some positive clinical results (Peitersen & Carlson, 1966; Smith, 1970; Stephens et al., 1982). Furthermore, glucocorticoids have been prescribed for the management of Meniere's disease (Hauser, 1959; Shea, 1983; Shea & Ge, 1996; Silverstein et al., 1998; Dodson et al., 2004; Doyle et al., 2004).

However, the results of clinical trials of pharmacotherapy of the inner ear vary widely. An illustrative case is that of amifostine, which demonstrated its capacity to protect against cisplatin-induced hearing loss in one study (Gurney et al., 2014), but did not result in a relevant therapeutic effect in another clinical trial (Fisher et al., 2004). Another example is steroids used to treat hearing loss. Meta-analyses of clinical trials conclude that the evidence for efficacy of steroids in idiopathic sudden sensorineural hearing loss is highly divergent (Conlin & Parnes, 2007; Plontke et al., 2022). One possible reasons for this variability could be the diversity of pathologies, as well as differences in administration strategies. Most drugs for inner ear therapy are administered systemically. To achieve sufficient drug bioavailability in the inner ear high drug doses have to be applied systemically, increasing the risk of adverse events. Next to this, the blood-labyrinth-barrier is not permeable for all kind of drugs (Förster et al., 2022). Local drug delivery presents an excellent solution for this challenge.

Current preclinical studies of local drug delivery methods to treat the inner ear include intratympanic, vestibular, and intracochlear applications. Among these methods, the intratympanic way is the most widely endorsed approach, considering as a compromise between application methods characterized by minimal invasiveness and optimizing the maximal entry of the active pharmaceutical ingredient into the cochlear. The tympanic cavity is connected to the inner ear via the round window niche (RWN) and its membrane (RWM). Drug diffusion from the middle ear to the inner ear is controlled by the permeability of the RWM. Intratympanic delivery is performed by liquids or drug-entrained matrices, such as gels (Coleman et al., 2007) and gelfoams (Ahmadi et al., 2019). However, these approaches have disadvantages, such as uncontrolled drug loading, uncontrolled diffusion through the RWM, outflow through the Eustachian tube, and no visual control of false membranes in the niche that impede or even prevent drug diffusion. These points lead to clinically relevant disadvantages due to ineffective drug diffusion. To address these issues, we propose an implant fitting in the patient-individually shaped RWN (Matin et al., 2021). Such a round window niche implant (RNI) can be additively manufactured, allowing unrestricted variability of shape and size so that the RNI fits in each anatomically individually shaped RWN. The printed material has to be flexible to allow an atraumatic insertion of the RNI in the RWN, which is surrounded by bone. Such an elastic RNI can be achieved by 3D-printing of silicone. The incorporation of drugs into the silicone prior to printing and sterilization enables precise drug loading. In relation to release kinetic studies, there is potential for giving knowledge which drug amounts are applied to the individual patient leading to precise knowledge on drug delivery to the inner ear in each specific patient. The proposed RNI could be implanted according to the patient's preference under general or local anesthesia. In either case, local anesthesia would be administered to the external auditory canal and the tympanic membrane to allow for a tympanomeatal flap. RNI implantation as part of such a tympanoscopy also allows obstructive fatty tissue or false membrane to be surgically removed from the niche before the RNI is placed there. This could further improve drug diffusion from the niche into the inner ear.

To prove the concept of RNI drug delivery for inner ear therapy, *in vivo* testing in preclinical models is required. Guinea pigs are a well-established animal model for hearing research (Naert et al., 2019) and are utilized in this study for validation of the RNI. The anatomy of the guinea pig ear allows easy surgical access to the cochlea (Albuquerque et al., 2009), and their hearing range (150–50 000 Hz) (Wever et al., 1963) overlaps with the hearing range of humans (20–20 000 Hz.) (Stebbins et al., 1982; Heffner & Heffner, 2007).

As a human-sized RNI does not fit into the round window area of the guinea pig, this study aimed to develop an appropriately sized RNI as a viable and effective drug delivery system for the guinea pig (GP-RNI). Dexamethasone (DEX) is widely used in preclinical studies and clinical trials to treat inner ear disorders. Therefore, DEX was selected for our investigation. We utilized imaging, segmentation, modeling, 3D printing, and tested the accuracy and precision of printing, biocompatibility, bio-efficacy and drug release of DEX-loaded silicone *in vitro*. The implantability and attachment to the RWM were evaluated in fresh guinea pig cadavers. Furthermore, we assessed the efficacy of the DEX-containing GP-RNI *in vivo* in a cochlear implant (CI)-trauma model. The application of DEX has been proven to be beneficial for preserving residual hearing and reducing fibrosis after cochlear implant surgery (Chang et al., 2009; Lee et al., 2013; Wilk et al., 2016). The efficacy of DEX delivery via GP-RNI was evaluated by measuring the residual hearing thresholds and fibrotic growth around the CI.

2. Materials and methods

In this study, all animals were Dunkin Hartley guinea pigs, including live ($N=14$) and cadavers ($N=23$). All experiments were conducted in accordance with the German Animal Welfare Law and the European Directive 2010/63. The cadavers ($N=12$, Charles River Laboratories, France) used to set up the GP-RNI design were generated as part of previous studies which were conducted with permission of the local authority (Lower Saxony State Office for Consumer Protection and Food Safety (LAVES), Oldenburg, Germany, registration number 19/3145 and 20/3502). The fresh cadavers ($N=11$) used for the implantability tests, imaging and grinding were kindly provided by the working group of Prof. Mazzouli-Weber (Department of Physiology, University of Veterinary Medicine Hannover, Foundation, Hannover, Germany).

The *in vivo* study on chronically implanted guinea pigs ($N = 14$, Charles River Laboratories, France) was conducted with the explicit permission of the responsible governmental authority Lower Saxony State Office for Consumer Protection and Food Safety (LAVES, Oldenburg, Germany), registration number 20/3592. The objective is to further assess the safety and bio-efficacy in a clinical trauma model. Guinea pigs serve as valuable animal models for hearing research due to the availability of quantitative assays for hearing function and similar normal-hearing frequency range to that of humans. The sample size was calculated using G-Power (with $\alpha = 0.05$, and power = 0.80). The animals were allowed to acclimate to the animal facility for two weeks prior to treatment and were housed within a meticulously controlled environment, characterized by regulated temperature and humidity levels. Moreover, a consistent 24-h light-dark cycle (14 h light, 10 h dark) was maintained to ensure a standardized living condition. All surgeries start around 8 o'clock in the morning, lasting approximately 3 h, minimizing deviation resulting from variations in surgery time (Bijarnia et al., 2015; Cederroth et al., 2020). Throughout the study, animals had unrestricted access to food and water to ensure their well-being. Animals will be euthanized immediately under the following conditions: significant neurological symptoms such as a pronounced tilt of the head that affects general well-being even after the 2nd postoperative day, severe facial paralysis leading to difficulty in food intake, refusal to eat, weight loss of ≥ 20% over more than 2 days or marked apathy. All experimental procedures strictly followed the guidelines of the German 'Law on Protecting Animals' and the European Communities Council Directive 2010/63/EU, which regulates the ethical use of animals for experimental purposes. All *in vivo* experiments were performed at Hannover Medical School's approved facilities from April 1, 2022 to June 1, 2022, conducted by Chunjiang Wei, Ziwen Gao and Verena Scheper.

2.1. Imaging and segmentation

Temporal bones from 12 adult male Dunkin-Hartley guinea pig cadavers (Charles River Laboratories, France), weighing 300–350 g, were imaged using a µCT Scanner (XtremeCT II, ScancoMedical AG, Brüttisellen, Switzerland) (Malfeld et al., 2022; 2022). The scanner works at fixed power of 1470 µA and the selected scanning protocol applied 90 ms integration time and a resolution of 17 µm. The data sets were converted into DICOM (digital imaging and communications in medicine) files and the RWN area was segmented manually using 3D Slicer™ version 4.11 (http://www.slicer.org) to build a 3D reconstruction of the RWN which corresponds to be the main body of RNI (Figure 1, upper right). The segmentation process was conducted based on the axial plane image. Within this image, the RWN can be readily distinguished due to its discernible grayscale contrast in comparison to the scala tympani (Figure 2(A)). The upper boundary of the segmentation is defined by a straight line connecting the edges of the round window's two ends (upper surface), while the lower boundary is determined by the RWM (lower surface) (Figure 2(B)). By filling the region between the upper and lower

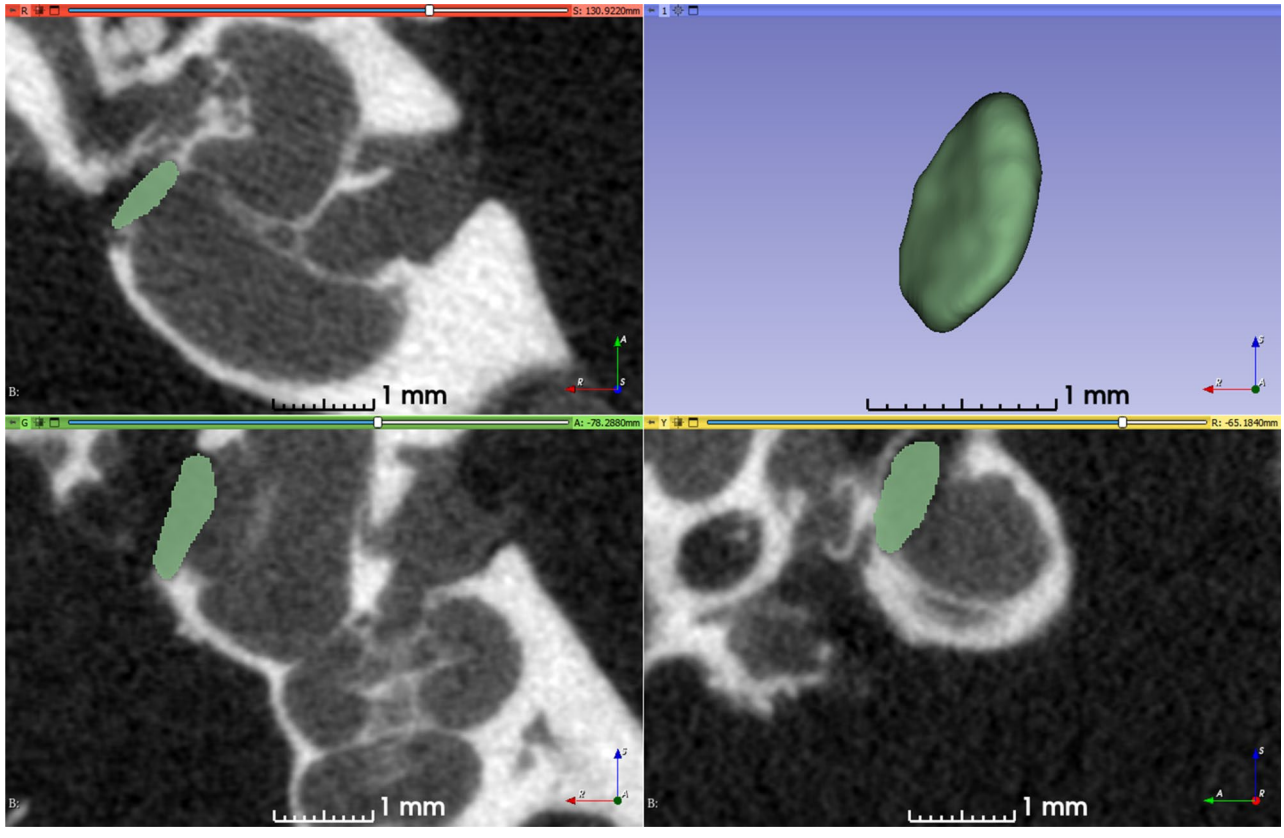

Figure 1. Segmentation of the RWN (green area) in 3D Slicer™. Axial (upper left), sagittal (lower left) and coronal (lower right) plane images of the segmented RWN and the 3D reconstruction of the RWN (upper right) that corresponds to the implant part of the GP-RNI.

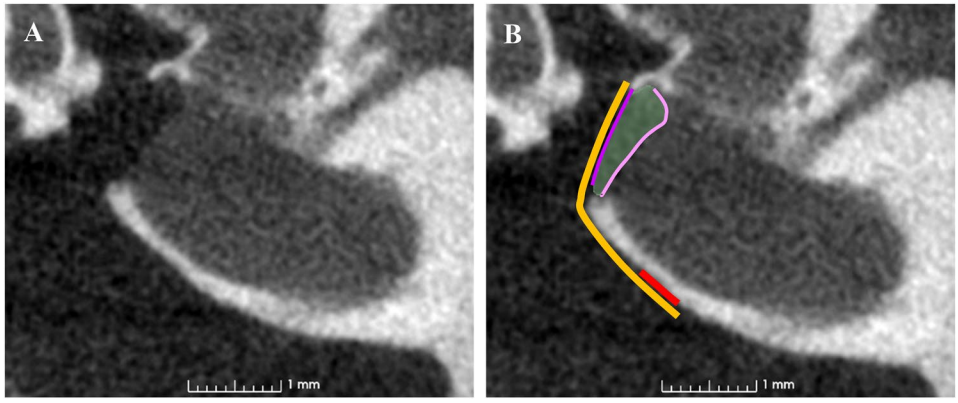

Figure 2. (A) A µCT Scan of a guinea pig cochlea. The RWN can be easily distinguished from the surrounding tissue due to the differences in density. (B) The graphic illustration of the designed GP-RNI model. The main body of the GP-RNI (purple and pink surrounded area) is equipped with a handle (yellow) which will be glued (red) onto the bony wall of the cochlea for fixation. For better illustration, we define the upper surface (pink) as the surface of RNI attached to the RWM and the lower surface (purple) as the one attached to the handle.

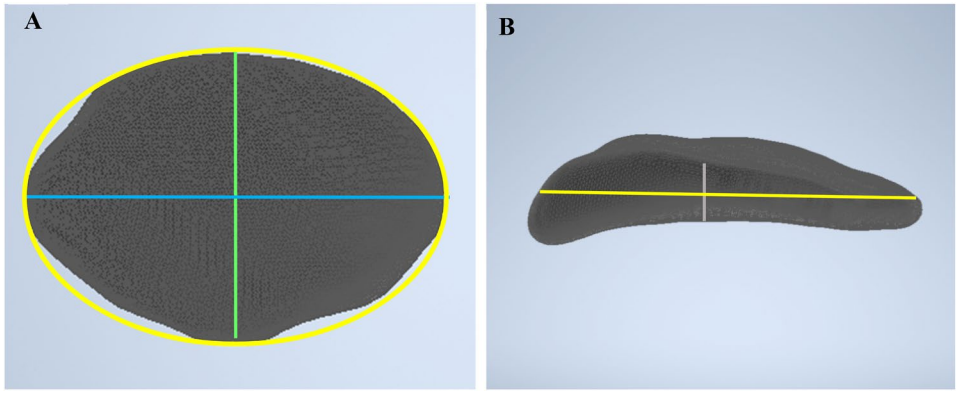

Figure 3. All dimensions of the main body of GP-RNI, which were measured for mean model design. Yellow: the Middle layer profile of the RNI; blue: long axis; green: short axis; grey: height.

boundaries, the segmentation of a single layer is completed. This procedure was repeated iteratively, starting from the initial layer where the RWN becomes visible, and continuing until the layer where it is no longer discernible. Finally, filling between slicers and the 3D reconstruction of the RWN was generated.

For better understanding the main body's shape and dimensions, which are essential for the subsequent implant design, important geometric information needs to be obtained. Since the profile of the segmented main body is similar to an ellipse, the characterization can be achieved through the determination of key geometric parameters. Specifically, the long axis and short axis of the middle layer, as well as the height of the main body, play a pivotal role in describing its morphology. The long axis is the longest diameter of an ellipse and the short axis is the shortest diameter of an ellipse. Each endpoint of the long axis is the vertex of the ellipse, and each endpoint of the short axis is a co-vertex of the ellipse. The center of an ellipse is the midpoint of both the long and short axis. The height is perpendicular to the middle layer and through the center (Figure 3(A,B)).

2.2. Design of the GP-RNI

Humans have a highly individually shaped RWN, suggesting that 3D printing, which allows maximum design freedom, is the appropriate method for producing patient-individualized human RNIs for local and precise drug therapy of the inner ear. Guinea pigs do not have an individually shaped RWN such as it is present in humans. Therefore, we decided for a one-size-fits-all GP-RNI model to reduce the variabilities in the animal model. The height, long axis and short axis of the individual RNI reconstructions were measured (Figure 3(A,B)) and an average model was drawn based on the mean values of the 12 data sets using 3D Slicer™. The implant surface was processed by applying the surface smoothing effect in 3D Slicer™ and exported as an STL (standard tessellation language) file. A handle, which additionally illustrates the orientation of implantation, keeps the GP-RNI in situ, and improves the handling of the implant during surgery was added (Figure 2(B)). The handle should cover the main implant body, i.e., the RNI part attached to the RWM. The thickness of the handle should be as thin as possible while not easily deformed, and the length should be extending downwards the bony cochlea to be foldable and easy to fix on the cochlea via glue (Dental UV-cement, Tetric EvoFlow®, Germany). To protect the middle ear ossicles, the handle is optimal to lean against the cochlear bony wall resulting in a specific angle between the main body and the handle. Various handle designs were explored in an endeavor to optimize their suitability for cochlear application, including fan-shaped, oval, and square, etc. Subsequent evaluation on cadaver temporal

bones determined the final handle design, as illustrated in Figure 2. Finally, the mean model of the main implant body and the designed handle were merged using Meshlab (version 2021.05) and the entire GP-RNI model was saved as an STL file.

2.3. 3D-printing of the GP-RNI and sample-blocks

Besides the GP-RNI shape, simple, well-defined sample-blocks were printed for biocompatibility and bio-efficacy tests. The blocks were constructed using Autodesk Inventor (Autodesk, Dublin, Ireland, 2022), with side lengths of 6×6 × 6 mm, weighing approximately 0.2 g and therefore in a range to be tested in accordance with the ISO guideline 10993-12:2021 (International Organization for Standardization, 2021) in 1 ml of medium. The 3D block model was saved as an STL file.

The RNIs and blocks were 3D printed using a 3D-Bioplotter® Manufacturers Series (EnvisionTEC GmbH, Gladbeck, Germany) equipped with a low-temperature printing head operated at a pneumatic pressure of 5 bar (GP-RNI) or 3 bar (blocks) and a UV Curing Head (365 nm). Silicone (60 A MG, BIO-83-6001, EnvisionTEC, USP Class VI grade) and its catalyst (catalyst compound, EnvisionTEC) were meticulously prepared in a ratio of 50:1. This preparation involved the use of a Speedmixer™ DAC 150.1 FVZ (Hausschild & Co.KG, Hamm, Germany), operated for 2 min at 3500 rpm. Subsequently, different concentrations of DEX (1%, 5%, 10%, or 20% w/w; Caesar & Lorentz GmbH, Hilden, Germany) were added to the silicone using the Speedmixer™ for an additional 2 min at 3500 rpm. For the histological evaluation, the GP-RNI was stained by adding one small drop of blue dye (SILC-PIG®, KauPo, Germany) to the silicone using the Speedmixer™ again for 2 min operated at 3500 rpm. The silicone/drug mix was loaded into 30 cm^3 polypropylene cartridges (Nordson Australia Pty Ltd., Sydney, Australia) attached with a 200 µm (GP-RNI) or 400 µm (blocks) dispensing needle tip (Nordson Australia Pty Ltd., Sydney, Australia). Then the STL files (GP-RNI or block) were loaded into the Perfactory RP software (EnvisionTEC GmbH, Gladbeck, Germany) and sliced. The sliced model was imported to Visual Machines software version 2.8.130r7 (EnvisionTEC GmbH, Gladbeck, Germany), where the GP-RNI was assigned an infill with a fiber spacing of 0.2 mm, while the blocks with a spacing of 0.4 mm. The needle movement speed of printing process is 1.6 mm/s, and the silicone cross-linked layer-by-layer through the application of UV light. After finishing the printing, the GP-RNIs and blocks need a 30-min UV irradiation (1800×100 µJ/cm^2; SpectroLinker XL-1000, Spectroline, Westbury, NY, USA) to eliminate microbiological contamination.

2.4. Accuracy and precision of printing

The evaluation of the printing quality consists, amongst others, of two aspects: accuracy and precision. The accuracy refers to how close a printed sample measurement is to the model we designed and the precision refers to how close repeated printing runs of the same object are to each other. All the tested samples were printed using only silicone. To measure the printing accuracy, the surface of the printed sample is sprayed with TiO_2 to make it x-ray dense. Subsequently, the GP-RNI was scanned using a 3D-Scanner (Zeiss Metrotom 6, ZEISS) and exported as an STL file. The STL files of the mean model and the scanned sample were compared using GOM Inspect Pro (ZEISS). Additionally, to evaluate the printing precision, twenty GP-RNIs were printed continuously, subsequently examined under a microscope to visualize shape differences and the weight of each sample was measured as an indicator of dimensional consistency.

2.5. Drug distribution in the printed silicone

DEX (Caesar & Lorentz GmbH, Hilden, Germany) was mixed with the silicone (20% w/w) using a Speedmixer™ at 3500 rpm for 2 min. Subsequently, the silicone containing 20% DEX was printed using the above described GP-RNI mean model STL file and the described printing process. The printed GP-RNI was scanned in an X-Ray microscope, the XRADIA Versa 620 (ZEISS). The voltage was 40 kV and the power was 3 W. A 4x objective and a LE 1 filter were used. The exposure time was 30 s per picture and 1601 pictures were made, which led to a scanning time of 14 h. To increase the contrast the distance between source and GP-RNI and the distance between sample and detector was doubled. To determine the DEX particle size, a spatula tip of pure DEX was placed on a glass slide and the DEX was visualized using a microscope (Olympus CKX41, Olympus, Japan). Images were taken and the particle size was measured using Olympus CellSens standard software (Olympus, Japan).

2.6. Biocompatibility and bio-efficacy tests

To test the biocompatibility and bio-efficacy of the 3D-printed, drug-containing, silicone sample-blocks, eluates were generated by incubating each sample (n = 3 per condition) in 1 mL artificial perilymph (1 mL distilled water with 8.4738 mg/mL NaCl, 0.2013 mg/mL KCl, 0.493 mg/mL $MgSO_4 \cdot 7H_2O$, 0.1764 mg/mL $CaCl_2 \cdot 2H_2O$, 1.1915 mg/mL HEPES and 1 mg/mL bovine serum albumin; pH = 7.4) in centrifuge tubes (Eppendorf, Hamburg, Germany; 2 mL capacity) for 72 h in an incubator (CB150; Binder, Tübingen, Germany; 37 °C, 5% CO_2, 95% humidity).

2.6.1. Biocompatibility

The cytotoxic effect of the printed DEX-silicone blocks was analyzed via MTT (3-(4, 5-dimethylthiazol-2-yl)-2, 5-diphenyltetrazoliumbromid) assay using mouse fibroblasts (NIH/3T3, German Collection of Microorganisms and Cell Cultures GmbH, Braunschweig, Germany; ATCC-Number: CRL-1658). In short, living fibroblasts reduce the MTT to formazan, which causes the color of the medium to change from yellow to purple. The color change is quantified by measuring the optical density using a microplate reader. To induce toxic effects on the cells the PC was additionally treated with dimethyl sulfoxide (DMSO, 0.1%, AppliChem GmbH, Darmstadt, Germany). Cells were incubated in a 96-well plate for 24 h (5% CO_2, 37 °C, 90% humidity) to form

a half-confluent monolayer. After the 24-h incubation period, the culture medium was aspirated from the wells. Each well was then treated with 100 µl of treatment medium containing the appropriate concentration of the sample extract, the negative control (cell culture medium), the positive control (0.1% DMSO). The cells were incubated for an additional 24 h under the same conditions (5% CO_2, 37 °C, 90% humidity). Prepare fresh MTT solution by dissolving it in Minimum Essential Medium (MEM) without supplements and without phenol red, to a concentration of 1 mg/ml. Sterilize the solution using sterile filtration with 0.22 µm syringe filters, and use it the same day. After examining the plates, carefully remove the culture medium. Add 50 µl of the MTT solution to each test well and incubate the plates for 2 h at 37 °C. Subsequently, remove the MTT solution by decanting, inverting the plate, and blotting it against clean paper towels. Add 100 µl of isopropanol to each well. Gently sway the plate for 5 min at room temperature, then transfer it to a microplate reader (BioTek Synergy™ H1 Hybrid Reader, Santa Clara, CA, USA) equipped with a 570 nm filter to read the absorbance, using 650 nm as the reference wavelength. Based on the ISO guideline 10993-12:2021 for biological evaluation of medical devices (International Organization for Standardization, 2021), cell viability below 70% can be considered as cytotoxic.

2.6.2. Bio-Efficacy

The bio-efficacy of the blocks was validated by a TNFα-reduction assay following the published protocols using DC2.4 mouse dendritic cells (DCs) (Sigma-Aldrich, St. Louis, MO, USA, LOT: 3093896) (Gao et al., 2021; Matin-Mann et al., 2022). The principle of this assay is to stress the cells by lipopolysaccharide (LPS) in order to stimulate the production of TNFα. The released DEX should lead to a reduction in the production of TNFα. 100 µL fresh medium including 0.5 µg LPS/mL (Sigma Aldrich, St. Louis, MO, USA) was added to all wells to induce stress, except for the NC (= seeded cells in the graph), lacking LPS to detect the baseline TNFα production of the DC2.4 cells. To each well, except the positive control (PC, TNFα production of LPS stressed cells), 50 µL eluate harvested from pure silicone or silicone containing 1%, 5%, 10% or 20% DEX, was added. The subsequent analysis for TNFα-concentration used an enzyme-linked immunosorbent assay (ELISA) kit (Mouse TNF-α ELISA Kit PicoKine, Boster Biological Technology, Pleasanton, CA, USA), performing in accordance with the manufacturer's instructions. All conditions were tested in triplicate.

2.7. Drug release

Dexamethasone was used as the reference substance for quantification of the drug for the release test. A 0.9% sodium chloride solution (sodium chloride obtained from Cealo & Loretz GmbH, Hilden, Germany) was used as the release medium. Ultrapure water obtained with a Astacus Reagent Ultra Pure Water System (membraPure GmbH, Bodenheim, Germany) served as the solvent for the sodium chloride solution.

For the release test, the implants were incubated for 29 d in 250 µL of the release medium. The release test was performed in 0.5 mL reaction vessels (ROTILABO®, polypropylene, colorless, with lid) at 37 °C and with shaking at 100 rpm (IKA® KS 3000 i control, IKA®-Werke GmbH & Co. KG, Staufen, Germany). To determine the theoretical loading of the implants, the masses were determined with a Sartorius SE2 balance (Sartorius AG, Göttingen, Germany) prior to the test. The investigation time points were 1 h, 6 h, 1 d, 3 d, 7 d, 10 d, 14 d, 17 d, 21 d and 29 d. After each time point, samples were removed from the reaction vessels, blotted on cellulose, and then transferred to reaction vessels containing fresh, pre-tempered release medium. The transfer of the samples was performed very carefully with low mechanical stress. The obtained release medium samples were frozen and stored at − 20 °C until analysis of the drug content.

To determine the amount of DEX released, liquid chromatography (LC) was used in combination with a mass spectrometry (MS) detector (LCMS-8060, Triple Quadrupole MS Shimadzu Corporation, Kyoto, Japan). The LC component (HPLC) consisted of a SIL-40C X3 autosampler, a LC-40B X3 solvent delivery module, a CTO-40S column oven, a SPD-40 UV-Vis detector and a FCV-20AH_2 valve unit. The system was equipped with a Kinetex Polar C18 column (150 × 2.1 mm, 2.6 µm, Phenomenex Inc., Torrance, CA, USA) connected with a SecurityGuard™ ULTRA Cartridge (Phenomenex, Torrance, USA) and a SecurityGuard™ ULTRA Holder (Phenomenex, Torrance, USA). A flow rate of 0.4 mL/min at 40 °C was selected as the parameter for the gradient method used (gradient conditions, see Table 1). The mobile phase consisted of water (LCMS grade; eluent A) and acetonitrile (ACN; eluent B), both mixed with 0.1% (V/V) formic acid. The total run time of the LCMS method was 13 min.

Samples were diluted in equal parts with a mixture of ACN/water (both containing 0.1% formic acid (V/V)) prior to measurement. An internal standard was spiked to each sample (prednisolone; target concentration 10 ng/mL). The dilution series of calibration standards were prepared in a mixture of ACN/water (+0.1% formic acid (V/V) (equal parts) and subsequently diluted with a 0.9% sodium chloride solution (equal parts) and spiked with the internal standard (prednisolone dissolved in ACN/pure water (+0.1% formic acid (V/V)). The injection volume was 10 µL.

In order to prevent contamination of the ionization unit, initially the eluent was directed to a waste bottle. For analysis of the samples, after 6 min the valve unit changed the direction of the flow to the mass spectrometer and after 8.55 min the valve switched back to its initial position. The retention times for DEX and prednisolone were about 7.2 min and 6.8 min respectively. The MRM (multiple reaction monitoring)

Table 1. Gradient conditions of the LCMS method with water (eluent A) and acetonitrile (eluent B) (both with 0.1% formic acid (V/V)), flow rate 0.4 mL/min.

Time (min)	Eluent A (%)	Eluent B (%)
0	80	20
4.5	80	20
7.5	10	90
10.0	10	90
10.5	80	20
12.0	80	20

Table 2. Summarized flow rates and temperatures of the LCMS method.

Parameter	Value
Nebulizing gas flow	3 L/min
Heating gas flow	10 L/min
Interface temperature	300 °C
Desolvation temperature	526 °C
Desolvation line temperature	250 °C
Heat block temperature	400 °C
Drying gas flow	10 L/min

transitions used for quantification and the corresponding collision energies for DEX were 393.3 -> 355.2 m/z (-12 eV) and for prednisolone 360.5 -> 147.1 m/z (-23 eV), respectively. The quantification range for DEX was between 2.33 and 931 ng/mL. Further used parameters (flow rates and temperatures) are summarized in Table 2.

For the data acquisition and analysis, Shimadzu software (LabSolutions, version 5.97 SP1) was used. Calibration curves were constructed by plotting the peaks area ratio of dexamethasone and the internal standard (prednisolone) against the concentration of dexamethasone. A $1/c^2$ weighted least squares linear regression was applied for the calculation of the concentration.

The LCMS method used was validated for linearity, accuracy and precision. Accuracy and precision were performed on four different DEX concentration ranges (Q1: 821.05 ng/mL, Q2: 410.52 ng/mL, Q3: 205.26 ng/mL and Q4: 45.61 ng/mL) using quality control samples (Q1–Q4) in five replicates.

2.8. Implantability

The implantability of the printed GP-RNI was evaluated by insertion into $N = 9$ fresh guinea pig cadavers (provided by the working group of Prof. Mazzouli-Weber) in a surgical procedure designed to simulate implantation in live animals. Whether printing variation affects implantability was tested in two additional right cochleae using implants with the highest and lowest weighing RNIs. All animals were implanted unilaterally in the right ear. Firstly, we used a scalpel to make an approximately 2–3 cm incision, positioned 3–5 mm posterior to the pinna. Following the palpation of the auditory bulla, we carefully cut the muscles in the retroauricular area using surgical scissors. The muscles were then dissected from the bulla and gently pushed aside. Subsequently, we used a retractor to fully expose the incision and carefully drilled a hole into the bulla to access middle ear by rotating the scalpel tip until the perforation was achieved. The bullostomy was then enlarged as necessary to ensure optimal visualization of the basal turn and RWN of the cochlea. By the use of a tweezer the upper part of the handle was grasped and the implant was placed on the round window. Subsequently, a probe was utilized to carefully adjust the orientation of the implant, ensuring that the handle could be adhered to the bone wall. Finally, gently insert the implant securely into the RWN. Moreover, the oval shape of the implant offered inherent advantages in terms of stability, as once correctly inserted, the implant resisted inadvertent movement. One drop of dental UV-cement (Tetric EvoFlow®, Ivoclar Vivadent, Ellwangen, Germany) was applied to fix the handle to the bone wall. The bullostomy was carefully closed with dental UV-cement. Finally, the retroauricular incision was closed in two layers to complete the surgical procedure.

2.8.1. µCT imaging

To evaluate the position of the implanted GP-RNI in situ µCT imaging was applied (XtremeCT II, ScancoMedical AG, Brüttisellen, Switzerland; for details see Section 2.1; $N = 7$). Six GP-RNI implanted guinea pig heads were scanned. The DICOM data sets were reconstructed using COMET (Lexow et al., 2016) and the position of the GP-RNI in the RWN was visually analyzed. Silicone possesses a higher density than air, allowing for its visualization through CT imaging. Following the implantation of GP-RNI in the RWN, the density of the previously low-density niche increased. Furthermore, in an effort to enhance the visualization of the GP-RNI and provide further clarity regarding its positioning in respect to the RWM, we added a small drop of contrast agent (Imeron®250, Bracco Imaging Deutschland, Konstanz, Germany) onto the surface of the GP-RNI to enhance its visualization, implanted it into a guinea pig RWN and subjected it to µCT scanning ($N = 1$).

2.8.2. Confocal laser scanning microscopy (CLSM)

The attachment between the GP-RNI and the RWM was assessed by scanning the cochlea of the six guinea pig heads mentioned above using CLSM. The cochleae were removed from the temporal bone, fixed in paraformaldehyde (PFA) for 1 h at room temperature, and then rinsed three times with phosphate-buffered saline (PBS) for 10 min each. Subsequently, the cochleae were decalcified in 10% ethylenediaminetetraacetic acid disodium salt (EDTA, Sigma-Aldrich Chemie GmbH, Schnelldorf, Germany) in PBS (pH 7.4) for three to four weeks, with regular EDTA changes every three days. After decalcification, they were rinsed three times with PBS for 10 min each. The cochleae were then dehydrated through a graded ethanol series: 70% ethanol overnight, 95% ethanol for 30 min, and absolute ethanol for 2 h. For refractive index adjustment, methyl salicylate benzyl benzoate (MSBB) was prepared by mixing five parts methyl salicylate with three parts benzyl benzoate (Merck KGAA). The cochleae were placed in a solution consisting of a 1:1 mixture of MSBB and absolute ethanol for 4 h at room temperature. The solution was then replaced with pure MSBB, and the cochleae were kept overnight at room temperature before being stored at 4 °C. Finally, the cleared cochlea was placed in MSBB and 3D-scanned using a Leica SP8 laser scanning confocal microscope (Leica Microsystems GmbH, Wetzlar, Germany), that emitted excitation wavelengths at $\lambda = 492$ nm for PFA-induced autofluorescence detection.

While the RWN in guinea pigs exhibit minimal variation, it is important to acknowledge that a singular average model cannot perfectly accommodate all individual variations. Hence, certain criteria are established to define an ideal average model. Specifically, the main body of the GP-RNI should adequately occupy the entire round window niche, while the upper surface of the implant should establish full contact with the RWM. To determine the conformity of the average

model, different z-stack cross-sections were examined, specifically focusing on the percentage of the implant area and the length of contact observed. If the average exceeds 90% in both measurements, this is considered as an accurate fitting.

2.8.3. Grinding

The GP-RNI was stained (see Section 2.3) and implanted in two fresh guinea pig cadavers (provided by the working group of Prof. Mazzouli-Weber). After the implantation of stained GP-RNI, the bulla was fully opened and the cochlea was extracted for grinding. Specimen Preparation, embedding and grinding were performed as described previously (Sieber et al., 2019). The specimen was fixed, followed with decalcification and dehydration (see Section 2.8.2). 0.1% Acid Fuchsin was added to enhance the contrast of the tissue against the embedding epoxy. The final step is embedding the specimen in epoxy resin (SPECI-FIX 40, STRUERS, Denmark). Grinding procedures were conducted using an AutoMet250 Grinder-Polisher (BUEHLER, Lake Bluff, IL, USA). Each layer was documented using a VHX-2000 measurement microscope (KEYENCE Corporation, Osaka, Japan) at 20x magnification.

2.9. In vivo test

The animal experiment was conducted to validate the potential biological effect of the DEX-loaded GP-RNI on inflammatory reactions in the cochlea. To assess this, cochleae were stressed by inducing a CI electrode insertion trauma, resulting in fibrotic tissue growth around the CI-electrode array and hearing loss (Wilk et al., 2016). Animals additionally implanted with a GP-RNI should hypothetically exhibit reduced fibrosis and have better (i.e., lower) hearing thresholds than CI-only-animals.

2.9.1. Animals, experimental timeline and medication

Fourteen adult Dunkin-Hartley guinea pigs (Charles River Laboratories, France), weighing between 300 and 350 g, received a unilateral cochlear implant (CI; MED-EL GmbH, Innsbruck, Austria) electrode insertion trauma followed by chronic CI insertion. Animals were randomly assigned to two groups, one with CI only (CI group) and one implanted, next to the CI, with a 1% DEX GP-RNI (CI + RNI group). The opposite, not implanted ears served as control.

On the day of surgery (day 0), the guinea pigs' frequency specific hearing thresholds (1, 2, 4, 8, 16, 32 KHz) were measured to confirm normal hearing (see Section 2.9.2). Subsequent implantation of CI and GP-RNI (see Section 2.9.3) and CT scan to check the position of CI and GP-RNI after surgery (see Section 2.8.1) were performed. After 4 weeks, on day 28, frequency specific hearing thresholds were measured again, followed by CT scanning to confirm if CI and RNI were still in situ. Finally, the guinea pigs were euthanized and the cochleae were extracted for histological analysis (see Section 2.9.3).

AABR measurement, implantation, μCT, and euthanasia were performed under general anesthesia, with all anesthetized animals positioned on a 38 °C heating mat. Prior to anesthesia, animals received a probiotic (oral 0.5 g Bene-Bac® Gel, Dechra Veterinary Products Deutschland GmbH, Germany) and sedation (oral diazepam, Diazepam-ratiopharm® 10 mg/mL Tropfen zum Einnehmen, ratiopharm GmbH, Germany) at 4 mg/kg. The inductive dose of general anesthesia included intramuscular medetomidinhydrochloride (Dormilan® 1 mg/mL, alvavet Tierarzneimittel GmbH, Germany) at 0.2 mg/kg, midazolam (Midazolam 5 mg/mL, PANPHARMA GmbH, Germany) at 1 mg/kg, and fentanyl (Fentadon 50 μg/mL, Dechra Veterinary Products Deutschland GmbH, Germany) at 0.025 mg/kg. Maintenance was achieved using half the initial inductive dose if necessary. Anesthesia was antagonized by subcutaneous injection of atipamezole (ATIPAZOLE 5 mg/mL, Prodivet pharmaceutics, Belgium) at 1 mg/kg and flumazenil (Flumazenil-hameln 0.1 mg/mL, Hameln pharma GmbH, Germany) at 0.1 mg/kg. To reduce pain and prevent infections, antagonization was conducted without naloxone to maintain the analgesic effect of fentanyl. Postoperative care included 0.2 mg/kg meloxicam (Metacam® 0.5 mg/mL, Boehringer Ingelheimmedica GmbH, Germany) for 3 days and 5 mg/kg enrofloxacin (Baytril® 2.5%, Elanco GmbH, Germany) by mouth for 7 days. Euthanasia was performed via intracardiac injection of no less than 300 mg/kg pentobarbital (Release® 300 mg/mL, Wirtschaftsgenossenschaft deutscher Tierärzte eG, Germany) by Chunjiang Wei, Ziwen Gao and Verena Scheper.

2.9.2. Acoustically evoked auditory brainstem response (AABR)

AABR tests were performed using a TDT System (Tucker-Davis Technology, Alachua, FL) in an acoustically- and electrically-shielded chamber. Acoustic stimuli were delivered through a calibrated loudspeaker (DT48, BeyerDynamic, Heilbronn, Germany), placed in the outer ear canal via a plastic cone. Using subcutaneous electrodes (CareFusion Nicolet, Middleton, WI, USA) to record AABR signals and analyzed with BioSigRP software. The lowest stimulus intensity of detectable AABR signal at specific frequency was considered the hearing threshold. Both ears of each guinea pig were tested on d0 and d28. The tested frequencies contain 1, 2, 4, 8, 16, 32, and 40 kHz. Only guinea pigs defined as normal hearing (thresholds ≤ 40 dB SPL) were able to be included in the study. More details could be found in previous publications (Scheper et al., 2019).

2.9.3. Surgery

After AABR measurement, all animals were implanted unilaterally in the right ear under general anesthesia (intramuscular medetomidinhydrochloride 0.2 mg/kg, midazolam 1 mg/kg and fentanyl 0.025 mg/kg). Areas of the skin to be incised received local anesthesia with prilocaine (Xylonest 1%, Aspen Germany GmbH, 0.5 ml, subcutaneous injection). The implantation procedures for CI and RNI were conducted as described in Section 2.8. Post-implantation, μCT was utilized to verify the position of the implants. Following antagonization, the guinea pig was placed under red light until it was totally awake and could maintain its body temperature.

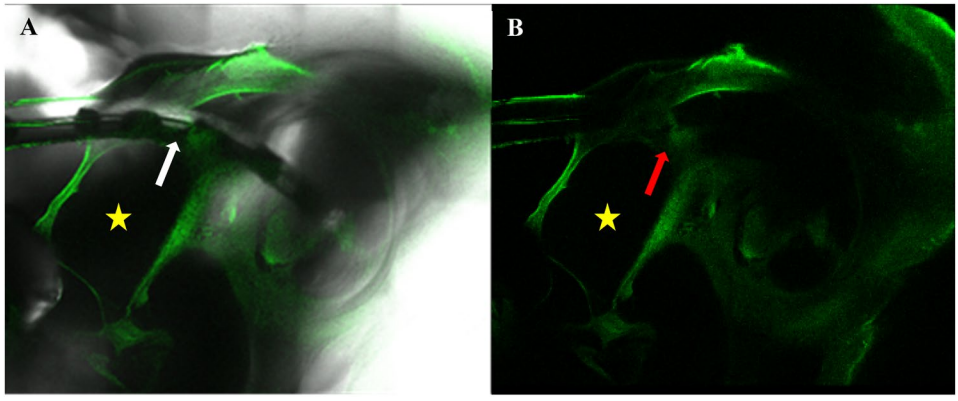

Figure 4. (A) One confocal laser scanning image of a CI-implanted cochlea (yellow star: scala tympani) with two channels opened, resulting in the visualization of the electrode (white arrow). (B) The same imaging as (A) but with only one channel opened. The green fluorescence shows the tissues fixed by the PFA, including the fibrosis (red arrow).

2.9.4. Histology

Tissue preparation of chronically implanted temporal bones followed the same protocol as described in Section 2.8.2. The evaluation of fibrosis around the CI was performed based on autofluorescence. The scanning of temporal bones used a Leica SP8 laser scanning confocal microscope (Leica Microsystems GmbH, Wetzlar, Germany) equipped with a white light laser providing an excitation wavelength of $\lambda = 492$ nm. The slices were generated utilizing z-stacks with 20 µm steps. The scanning parameters included a scanning speed of 400 Hz, 5× line averaging and 3× frame averaging, while the second channel TLD (brightfield detector/through the lens detector) was activated to visualize electrodes (Figure 4).

To analyze the filling of the scala tympani with fibrotic tissue as response to the electrode insertion trauma, each implanted cochlea was analyzed at 4 cross-sections of the scala tympani: the round window (RW) area, lower basal turn (LB), middle basal turn (MB) and upper basal turn (UB), using the Leica Confocal Software (LAS X Science Microscope Software; version LAS X 3.5.7.23225). The tissue response in each cross-section was assessed using a ranking score (Table 3) describing the percentage of filling of the respective cross-sectional scala tympani area as described previously (Behrends et al., 2023).

2.10. Statistical analysis

Statistical evaluations were performed using GraphPad Prism® version 8.4.3 (GraphPad Prism Software Inc., La Jolla, CA, USA). Before data analysis, a test for normal distribution using Shapiro–Wilk test was needed. For data analysis of biocompatibility, using an unpaired t-test to analyze the differences between groups. Bio-efficacy of the supernatants was analyzed by applying Kruskal–Wallis followed by Dunn's multiple comparison test. Hearing thresholds and fibrotic growth were analyzed using unpaired t-tests or Mann–Whitney tests based on the result of the normality test. P-values below 0.05 were considered statistically significant.

Table 3. Ranking score for fibrotic growth in the cochlea.

Ranking score	Fibrotic growth (X) (%)
0	none
1	$X < 25\%$
2	$25\% \leq X \leq 50\%$
3	$50\% < X < 100\%$
4	$X = 100\%$

Table 4. Overview of the accuracy (recovery) and precision (coefficient of variation) ($N = 5$) of the LCMS method used based on the quality control samples Q1–Q4.

Quality control sample	Nominal concentration (ng/mL)	Accuracy: Recovery (%)	Precision: Coefficient of variation (%)
Q1	821.05	98.1	0.8
Q2	410.52	101.2	1.4
Q3	205.26	101.5	1.8
Q4	45.61	107.5	1.6

3. Result

3.1. One-size-fits-all GP-RNI model

Twelve RNIs based on guinea pigs' anatomy were 3D reconstructed individually. The measurements of the long axis, short axis, and height were obtained via 3D slicer (Figure 3(A,B)) and the mean ± the standard deviation (SD) are reported (Table 5). Analysis of the data revealed minor differences among guinea pigs, which were lower than the horizontal and vertical printing resolution (0.2 mm). Therefore, a one-size-fits-all GP-RNI model was selected to reduce the variability in the animal model. The average model was designed using the mean values of the 12 data sets with a mean long axis of 1.30 mm, a short axis of 0.96 mm and a height of 0.35 mm.

Based on the requirements (see Section 2.2), the final design of the handle is presented below (Figure 5). The total length of the handle was 3.5 mm, which covers the whole RNI body and leaves enough space for handling and gluing and the thickness was 0.32 mm. Furthermore, to facilitate appropriate implant orientation, the angle between the long axis of the RNI and the midline of the handle is set at 130°,

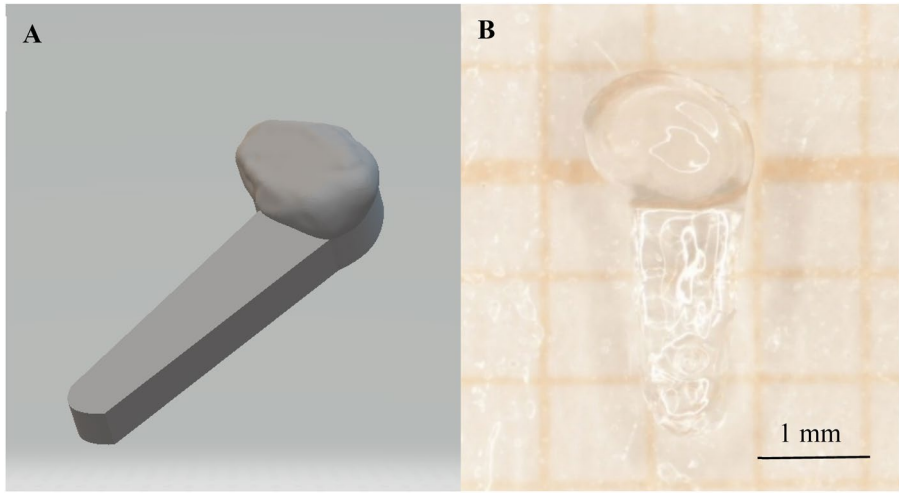

Figure 5. (A) Screen shot of the STL file of the mean model of the GP-RNI. (B) Example of a 3D-printed drug-free silicone GP-RNI.

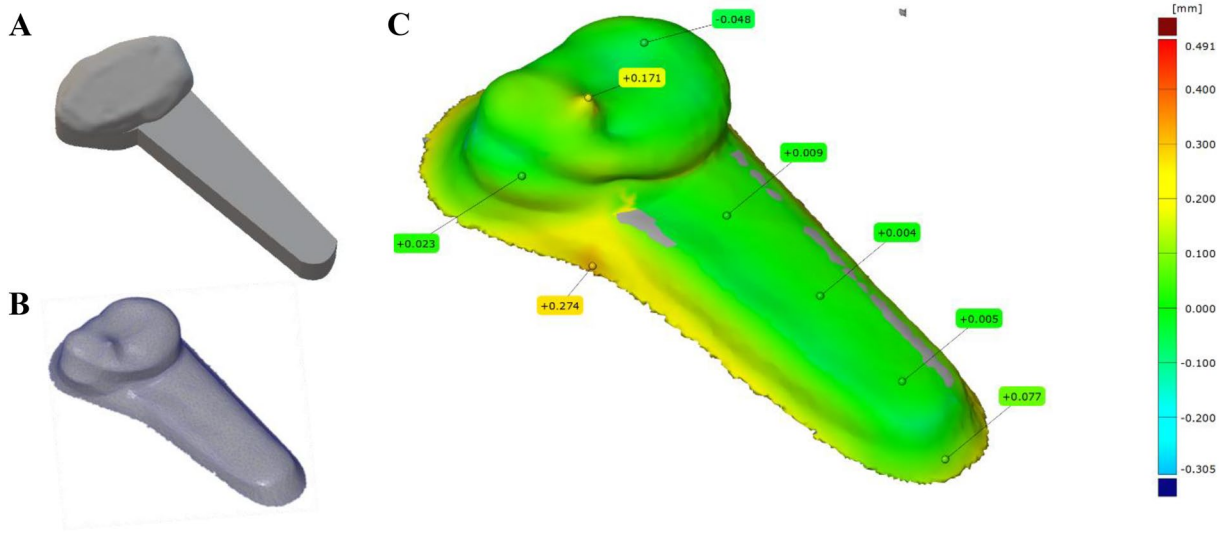

Figure 6. (A) The mean model of the GP-RNI (STL file). (B) The resulting surface scan of a printed GP-RNI (STL file). (C) Surface comparison of printed (B) and planned GP-RNI (A). The overall difference is green, most with less than 0.1 mm difference between planned and printed sample. Seven points on the surface were randomly selected and the specific differences were measured. A prominent observation is that the difference value of a little 'nose' in the main body is 0.171 mm, which is sometimes not avoidable when printing the last layer and nicely illustrates how important quality control is.

thereby ensuring secure fixation of this RNI-handle-transition region at the bony cochlea wall. Next to ensuring fixation to the cochlea, the angle helps the surgeon to find the correct direction of RNI positioning during implantation.

3.2. Accuracy

To evaluate the accuracy of the printing, the design model and the printed GP-RNI are compared through surface comparison. The surface scan of the printed model resulted in an STL file (Figure 6(B)) which was overlaid (Figure 6(C)) by the design model STL file. The visual inspection of the surface scan of the example shown in Figure 6(B) depicts a more round structure and a flattened bottom of the handle of the printed sample compared to the nominally planned GP-RNI (Figure 6(A)). Next to this, a little 'nose' is seen in the printed sample. The comparison results are color-coded depending on the difference. In case the printed GP-RNI is smaller than the planned design the color tends to blue, if both are the same size, it is green, and if the printed sample is larger than the GP-RNI model was designed to be, the color is red. The overall difference is green, with less than 0.1 mm difference between planned and printed sample. Randomly selected seven points on the surface and the specific differences are shown in Figure 6(C).

3.3. Precision

The precision evaluation involved an analysis of the weight for each printed sample ($N = 20$, Figure 7(A)). The GP-RNIs weight 1.019 ± 0.021 mg (mean $\pm$ SD). The first three printed samples vary from 1.06 to 0.97 mg (Figure 7(B)). When excluding those first samples the mean and SD is 1.02 ± 0.015 mg, which indicates the reliability and consistency of the printing

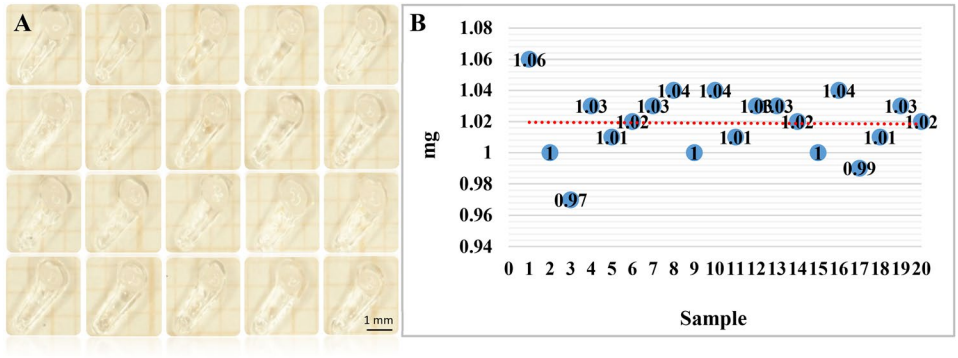

Figure 7. (A) Images of the 20 printed GP-RNIs analyzed for precision. (B) Weighting the 3D-printed samples shows that sample 1 and 3 are not in line with the other 18 samples. In total, the printed GP-RNIs weighted 1.019 ± 0.021 mg (mean ± SD). The red dotted line represents the average weight of 20 printed GP-RNIs.

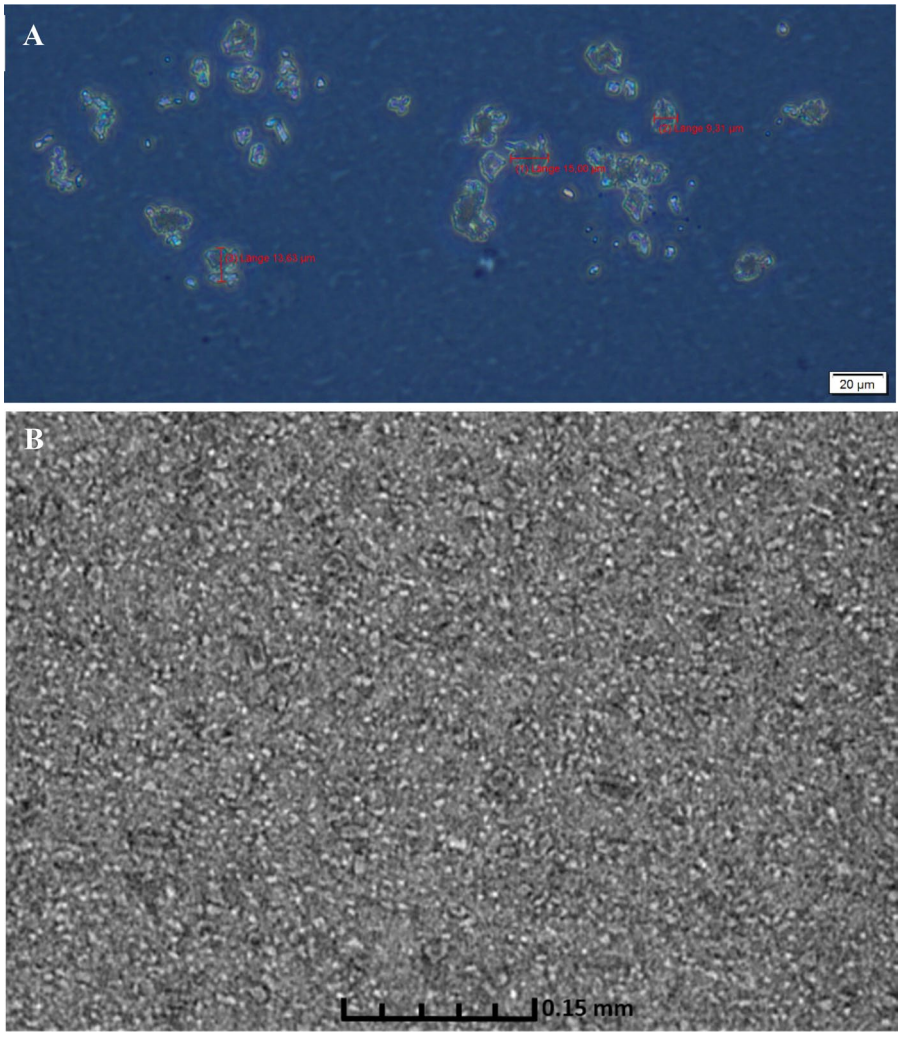

Figure 8. (A) Light microscopic image of pure DEX particles illustrating the size and form of DEX without mixing in any material. According to the manufacturer's information, this batch of DEX has a particle size of 99% <0.03 mm which is in accordance with the measured diameters of three randomly selected particles which are all smaller than 30 µm (scale bar: 20 µm). (B) Image of the 20% DEX containing GP-RNI showing homogeneous distribution of DEX (white particles) throughout the printed silicone (scale bar: 150 µm).

process, thereby validating the precision of our printing process. In addition, the minimum weight (0.97 mg) and the maximum weight (1.06 mg) have been tested in guinea pig cochlear specimens and confirmed to be still implantable, suitable and attaching the RWM. For quality control, we define the acceptable tolerance as 1.02 ± 0.02 mg.

3.4. Drug distribution

DEX particles without silicone were microscopically imaged. The diameters of the particles were measured and the randomly selected particles exhibited dimensions smaller than 0.03 mm (Figure 8(A)), which was consistent with the particle

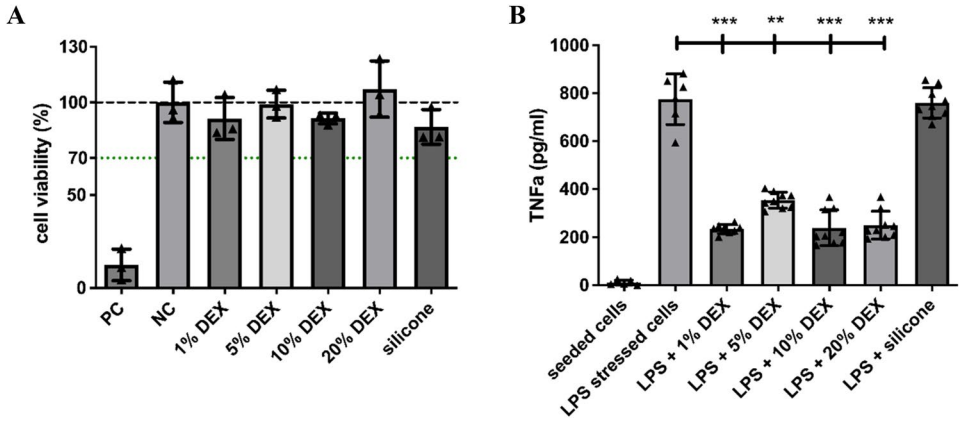

Figure 9. Results of the MTT test and TNFα reduction assay. (A) The MTT test showed no cytotoxic effect of 3D printed silicone with and without DEX. They are above the 70% viability level, which is according to the DIN EN ISO 10993-5 defined as the border for a cytotoxic effect (indicated as dotted green line). (B) The TNFα assay proves a significant reduction of TNFα for silicone containing DEX compared to the positive control (PC, LPS stressed cells). No differences between the different DEX concentrations in silicone were detected (**$p < .01$; ***$p < .001$).

size data of this batch of drugs (information provided by the manufacturer).

The drug distribution within the 3D-printed 20% DEX containing GP-RNI was visualized by an X-Ray microscope. DEX is distributed as shown by the white particles in Figure 8(B). The images indicate that the distribution of DEX within the silicone is homogeneous. This result verified that the drug is evenly dispersed throughout the silicone, which is essential for ensuring consistent and reliable drug delivery from the implant.

3.5. Biocompatibility and bio-efficacy

The result of biocompatibility is as depicted in Figure 9(A). In comparison to the negative control (NC), the positive control (PC) showed a significant reduction in cell viability, indicating the successful experimental setup. The addition of eluates of pure silicone (95 ± 9%) and silicone with DEX showed no statistically significant impact on cell viability when compared to the NC (100 ± 11%). This observation suggested that both pure silicone and silicone containing up to 20% DEX can be characterized as biocompatible.

A TNFα-reduction test was used to evaluate the anti-inflammatory efficacy of the released DEX and the results are illustrated in Figure 9(B). Cells without stress (NC) exhibited a minimal TNFα-production (0.005 ± 0.0007 pg/mL TNFα/cell density), while this level significantly increased with the addition of LPS (PC) to 0.3 ± 0.05 pg/mL TNFα/cell density. In the pure silicone, the TNFα level (0.27 ± 0.03 pg/mL TNFα) resembled that of the PC and showed a significant increase compared to the NC. The drug released from the silicone containing DEX samples resulted in a reduction of TNFα levels, with cellular stress not significantly different from the NC.

3.6. Drug release

The LCMS method used was checked for linearity and had a coefficient of determination (R^2) of 0.9968. The accuracy and precision of the method were investigated using the quality control samples (Q1-Q4). Accuracy was assessed by recovery and precision by coefficient of variation ($N = 5$ each), which are shown in Table 4.

Table 5. Measurement of the GP-RNI dimensions ($N = 12$).

Dimensions	Length (mean ± SD)
Long axis	1.30 ± 0.017 mm
Short axis	0.96 ± 0.020 mm
Height	0.35 ± 0.017 mm

The recovery remained at a deviation of less than 2% for quality control samples Q1, Q2 and Q3. The quality control sample Q4 showed a deviation of about 7.5%.

The coefficient of variation remained below 2% for quality control samples Q1, Q2, Q3 and Q4.

The masses of the six investigated implants varied between 0.885 mg and 1.023 mg, which at a theoretical DEX content of 1%, contained on average of 9.66 µg (SD ± 0.46 µg) DEX. The release profile of the active ingredient DEX can be found in Figure 10(A) and the average amount of active ingredient released per release interval in Figure 10(B). An average of 0.01 µg (SD ± 0.01 µg) of DEX was released after 1 h and an average of 0.05 µg (SD ± 0.01 µg) after one day. Within the study period, an average of 0.35 µg (SD ± 0.07 µg) of DEX was released, which corresponds to a released amount of 3.6% of the theoretical initial drug loading.

3.7. Implantability

The RWN was microscopically visualized via a posterior approach (Figure 11(A)). The GP-RNI insertion was easy to perform by following the procedures mentioned above (see Section 2.8). After the implantation, the bulla was extensively opened and it was visually verified that the GP-RNI stayed in place after handling the guinea pig and the bulla for tissue preparation and did not touch or even damage other structures, i.e., the middle ear ossicles (Figure 11(C)).

3.7.1. µCT imaging

Following CT scans of six fresh guinea pig cadavers, the placement of implants within the RWN was successfully identified. However, the attachment of the RNI to the RWM was

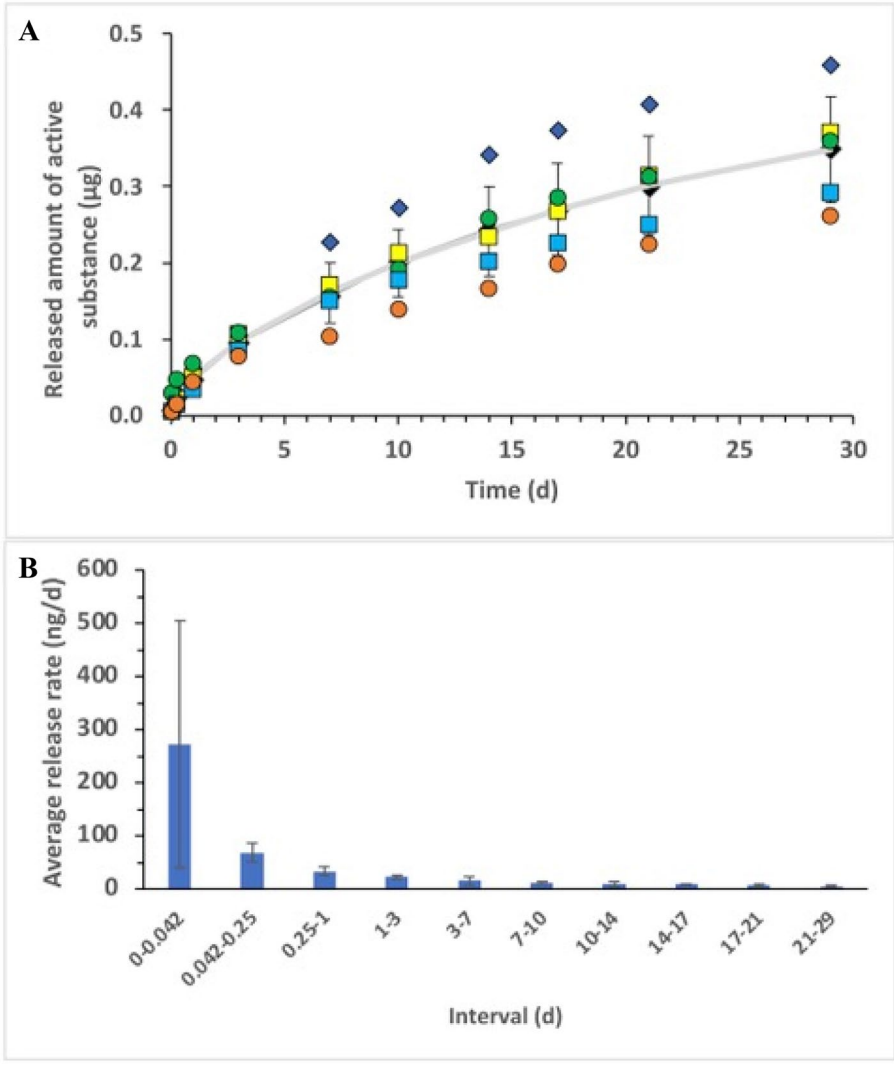

Figure 10. (A) Cumulative amount of DEX released from implants within 29 days ($N = 6$). (B) Average amount of DEX released from implants per day, within sample intervals. For a and B data are given as means ± SD.

Figure 11. Representative microscopic images of the RWN (A) and GP-RNI in situ (B). (C) Image of an implanted RWN after opening the bulla for tissue harvesting and analysis of GP-RNI placement (GP-RNI: circled in green). The main body of GP-RNI was well inserted into the RWN and the handle was correctly fixed on the bony wall (the blue dotted line is the boundary between the handle and the main body of the GP-RNI).

hardly possible to analyze due to the similarity in densities between silicone and the scala tympani (Figure 12(A)). After application of the contrast agent-covered RNI, the RNI and scala tympani can be distinguished, but the edge of the RNI cannot be clearly seen due to the scattering of the contrast agent (Figure 12(B)). Consequently, it is imperative to note that CT scanning serves primarily as a reliable tool for confirming the implantation of the RNI within the RWN, while its capability to assess the precise attachment of the RNI to the RWM remains limited.

3.7.2. CLSM

The 3D reconstructions of the implanted RWNs were used for evaluating the adhesion of the GP-RNI on the RWM. The

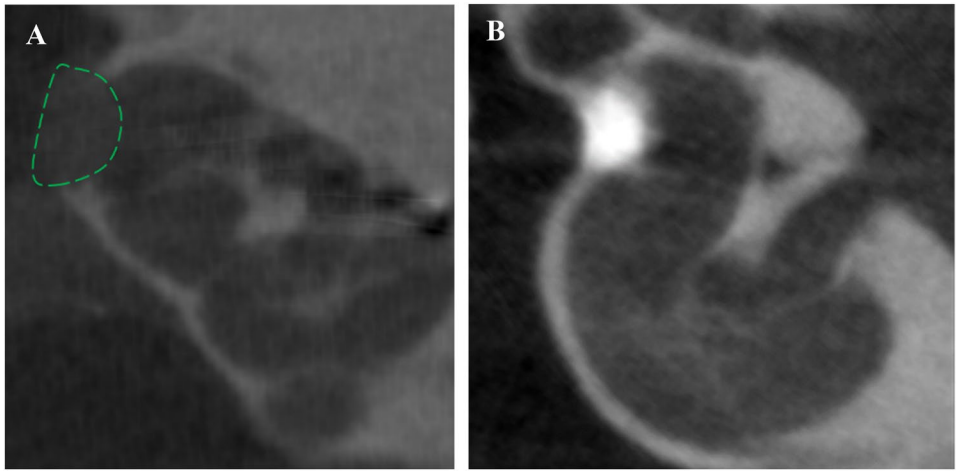

Figure 12. Exemplary µCT 2D images of GP-RNI implanted RWNs. (A) An implanted cochlea with a pure silicone GP-RNI (circled in green). (B) An implanted RWN with a GP-RNI covered with contrast agent.

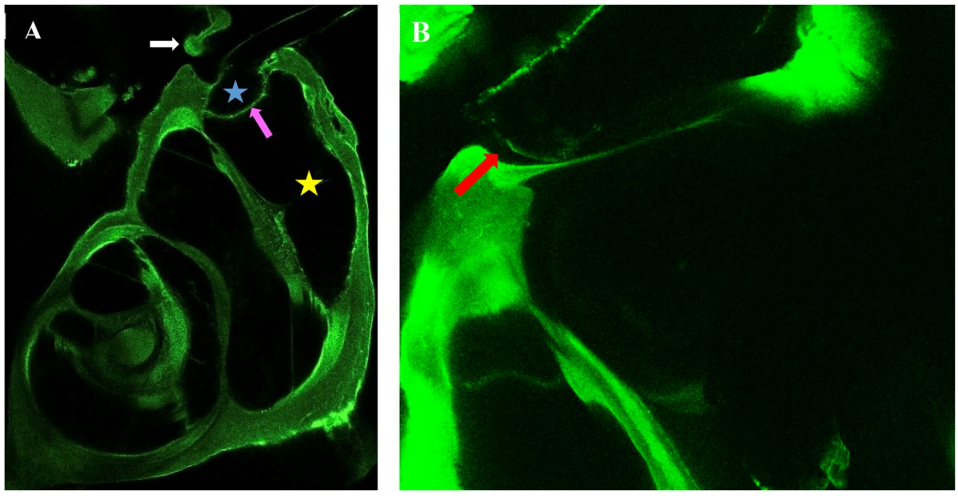

Figure 13. Confocal laser scan of an implanted cochlea. (A) The RWM (pointed by a pink arrow), GP-RNI (blue star) and part of the ossicles (pointed by a white arrow) can be seen, the GP-RNI is located in the RWN and well attached to the RWM (yellow star: scala tympani). (B) A z-stack image of an implant not fully attaching all RWN boundaries. As indicated by the red arrow, there is a gap between the RNI and the RWN.

analysis revealed that the entirety of the implant was appropriately positioned in the RWN, with the upper surface of the implant displaying complete contact with the RWM. However, certain z-stacks revealed that the GP-RNI did not achieve a perfect fit in the RWN. This observation was corroborated by the presence of a gap between the GP-RNI and the round window, as indicated by the red arrow in Figure 13(B).

3.7.3. Grinding

Figure 14 illustrates a section of the temporal bone showing the attachment of a GP-RNI and RWM. A thorough examination of the RWM at all layers affirmed its intact condition and the good attachment of the GP-RNI to the RWM. However, it is important to acknowledge a minor protrusion present on the upper surface of the RNI, resulting from detachment of the printing needle off the final implant. Consequently, this protrusion led to a localized deformation of the RWM at the point of contact. Subsequent observation confirmed that the GP-RNI neither contacts the ossicles nor affects the integrity of the RWM.

3.8. In vivo tests

3.8.1. Hearing threshold

All guinea pigs were normal hearing (<50 dB SPL) at the beginning of the experiment with no threshold differences between left and right ears (Figure 15(A,B)). After 28 days, one object from CI group and two objects from CI + RNI group were excluded from the analysis due to electrode failure, resulting in $N = 6$ animals in the CI group and $N = 5$ animals in the CI + RNI group. On the not-implanted side (left ears), the mean hearing thresholds (mean ± SEM) were increased by 2 ± 1 dB (CI group) and 4 ± 3 dB (CI + RNI group), showing that there were no significant differences in hearing thresholds between the control ears of the groups over the experimental period of 28 days (Figure 15(A)).

To illustrate the hearing loss caused by CI electrode insertion trauma and chronic CI implantation for 28 days Figure 15(C) depicts the mean hearing threshold of the CI implanted ears before (d0) and 28 days after CI insertion. The hearing threshold was significantly increased at the middle and higher frequencies of 8, 16, 32 and 40 kHz

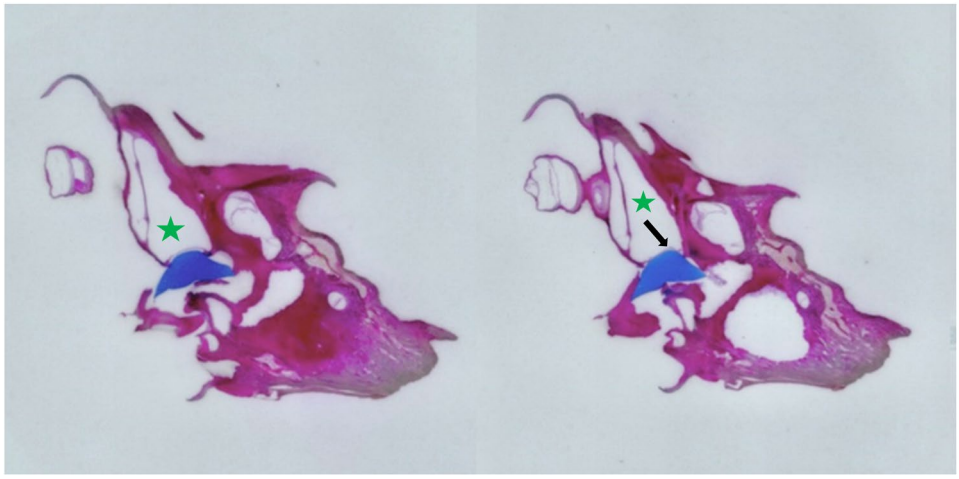

Figure 14. Images of grinded specimen of an implanted cochlea at 20x magnification. A section of the temporal bone, which was stained with acid fuchsin, visually represented in magenta. The blue depicts the stained GP-RNI, with its handle situated in the Middle ear cavity, while the main body is located in the RWN, and the upper surface well attached to the RWM. (green star: scala tympani, black arrow: protrusion).

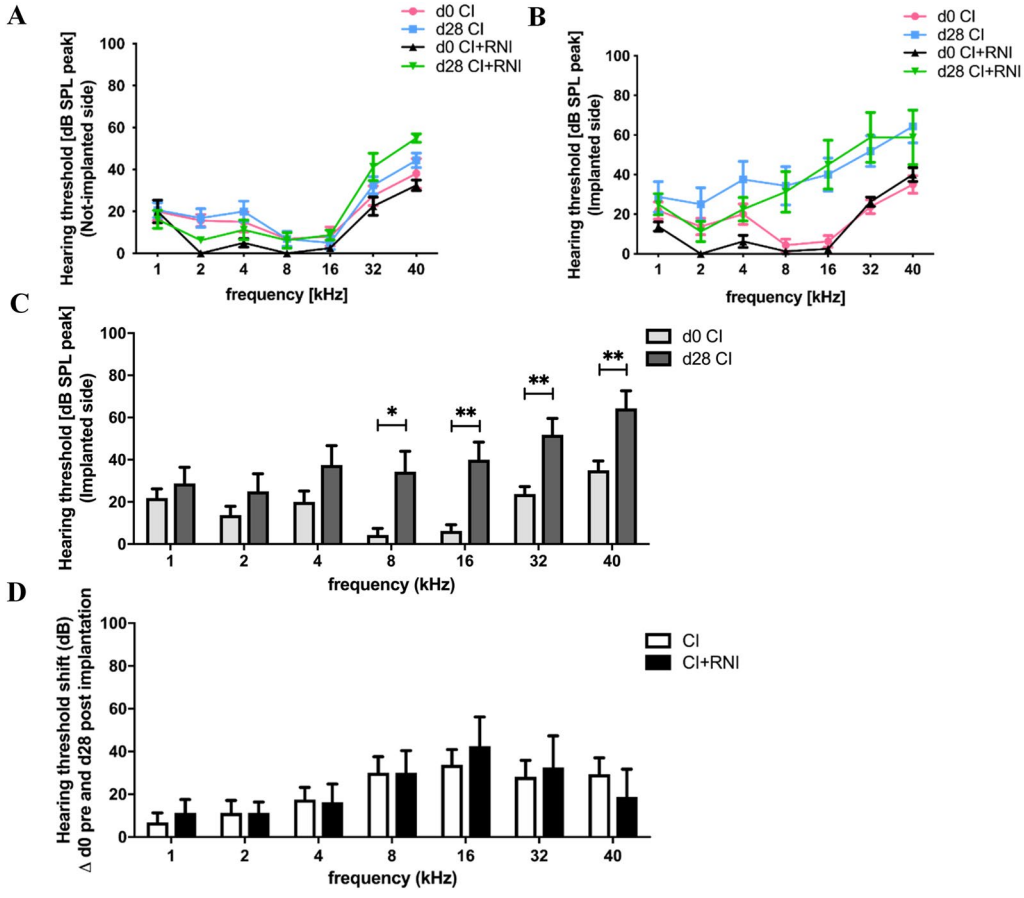

Figure 15. Mean frequency-specific hearing thresholds (mean ± SEM) of the (A) not-implanted side (left ears) and (B) implanted side (right ears) in both the CI and CI + RNI groups on day 0 (d0) and day 28 (d28). (C) The frequency-specific hearing threshold shift (threshold change from day 0 to day 28, mean ± SEM) of the implanted side in the CI group, showing significantly increased hearing threshold at 8, 16, 32 and 40 kHz. (D) The frequency-specific hearing threshold shift of the CI group and the CI + RNI group on the implanted side are plotted. No significant difference between the two groups are observed. (*$p < .05$; **$p < .01$).

compared to d0 (Figure 15(C)), indicating that the CI-trauma model was sufficient.

Comparing the hearing threshold shift on the implanted side between the CI and CI + RNI groups, no differences were detected (Figure 15(D)). The mean hearing threshold shift (mean ± SEM) of the implanted side between the CI group and CI + RNI was 4 ± 2 dB (1 kHz), 0 ± 1 dB (2 kHz), −1 ± 3 dB (4 kHz), 0 ± 3 dB (8 kHz), 8 ± 6 dB (16 kHz), 4 ± 7 dB (32 kHz), and −10 ± 5 dB (40 kHz).

3.8.2. Histology

The fibrotic growth around the CI only occurred in the basal turn (region from LB to UB), no fibrosis was observed in the

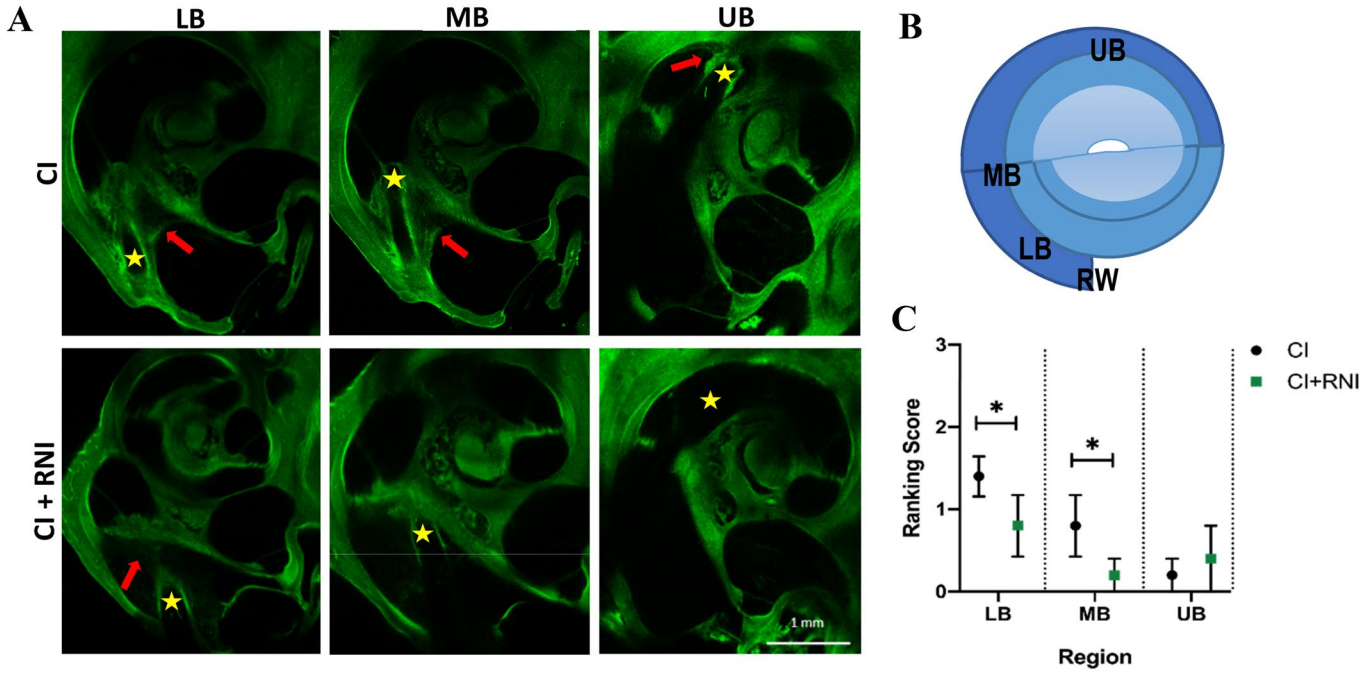

Figure 16. (A) Confocal laser scan of different cochlear regions in CI and CI + RNI groups at 10x magnification (yellow star: electrode, red arrow: fibrosis). (B) 4 cross-sections of the cochlea, including the round window area (RW), lower basal turn (LB), Middle basal turn (MB) and upper basal turn (UB) were analyzed for their percentage filling with fibrosis. (C) Evaluation of fibrotic growth in different cochlea regions. In region LB and MB, the CI + RNI group has lower ranking scores (mean ± SEM) than the CI group, while no significant difference is observed in the UB region between the CI and CI + RNI group. (*$p < .05$).

RW region of the scala tympani. The LB region, close to the cochleostomy, exhibited the most fibrotic growth, and from the LB region to the UB region, the fibrosis gradually decreases. The fibrosis in the LB and MB region in the CI + RNI group was significantly lower than in the CI group. No significant difference between the CI and CI + RNI group is observed in the UB region (Figure 16(B)).

4. Discussion

In this study, we established a RNI for local inner ear drug delivery in the guinea pig. The design of the GP-RNI is based on the guinea pig mean RWN anatomy. Many studies have revealed the structure and composition of the round window and the RWM in guinea pigs (Gan et al., 2013; Watanabe et al., 2014), while the volume and shape of the guinea pig RWN is rarely reported. Through segmentation, 3D reconstruction and measurement of the diameter and volume of 12 µCT scans, we found that the anatomy differs little among adult guinea pigs of the breed used (Dunkin Hartley, C. River). Therefore, to reduce the variabilities in the animal model, we suggest using this one-size-fits-all RNI for pharmacology studies in guinea pigs. It has to be noted that this mean model may not be the optimal one for other breeds, which may have smaller, larger, or individual RWN to which a drug releasing RNI has to be adapted. If our GP-RNI fits to other breeds as well has to be evaluated in future studies.

Due to its small size, the GP-RNI can be difficult to handle during implantation procedures. To overcome this limitation, we have designed and added a handle to the device. The handle not only facilitates gripping of the GP-RNI during *in vivo* experiments but also enables the surgeon to orient the device correctly during the implantation procedure which is relevant since the niche is, even though not individually shaped, not a circle but more an oval. In addition, the use of a biocompatible glue at the handle ensures secure fixation of the device in situ. The design of the handle was optimized after evaluating various shapes and angles. Parameters, such as the volume, ease of clamping and insertion, and the potential for damage to adjacent structures, such as the middle ear ossicles, were considered during the design process. Several *in vitro* and cadaveric tests were performed to assess the efficacy and safety of the handle design before finalizing the current design. The addition of the handle to the GP-RNI represents a significant improvement that enhances the usability and safety of the device during *in vivo* experiments.

The GP-RNI is manufactured using 3D printing of liquid silicone, crosslinked by subsequent UV-exposition. Except for this, the RNI can also be manufactured by micro injection molding of silicone. This is a two steps process with molds being 3D-printed based on the mean guinea pig RWN model using digital light processing and subsequent injection of silicone, which cures as temperatures decrease (Mau et al., 2023). Finally, the molded specimens have to be post-processed by removing the in- and out flow structures. Compared to molding, the jetting process used in the present study is a one step process via direct printing of the implant, no post-processing is needed, saving time and material and therefore money, which all is crucial for the further clinical translation of a human RNI. For printing quality control, the accuracy and precision of the 3D printing needs to be confirmed. By comparing the surfaces of the STL file of the nominal mean model and the printed GP-RNI, an overall match was observed. The precision test yielded promising results, demonstrating a notable level of

consistency in the printing process. Nevertheless, it is important to acknowledge that there remains a possibility of producing RNI samples that do not meet the printing tolerance (see Section 3.3). Therefore, it is imperative to conduct thorough assessments by weighing and examining the prints using a microscope to ensure their quality. It should be noted that this value of weight is only applicable to pure silicone printed RNI. The addition of different drugs and their respective concentrations can potentially alter this value, necessitating the need for subsequent measurements and reevaluation. Furthermore, future investigations may involve evaluating additional factors such as hardness, viscosity, and other relevant properties of the prints. These parameters hold potential as sensitive indicators for assessing printing quality, as they can be influenced by the incorporation of different drugs or variations in drug concentrations.

To determine if the 3D printed model fits all guinea pigs from our laboratory's breed, we unilaterally tested it on 6 fresh cadavers. The results of the implantation revealed its suitability in the used animals. Initially, we conducted a µCT scan as part of the evaluation. While the GP-RNI was discernible in the µCT scan, detailed observation of the attachment between the GP-RNI and the RWM was challenging due to the limited resolution of the µCT scan in accurately identifying these structures. We conclude that µCT scans of resolution as used in this study are primarily suitable for providing a rough understanding of the general placement of the RNI in situ. In our study, it does not facilitate precise assessment of the intricate attachment between the RNI and the RWM. Through the utilization of CLSM, distinct images of the RNI and RWM were obtained, providing a more meticulous evaluation. The CLSM indicated that the entire implant was appropriately positioned in the RWN, with the upper surface of the implant well attached to the RWM. However, certain z-stacks unveiled that the RNI in some cases did not achieve an optimal fit within the RWN, manifesting as the presence of gaps between the RNI and the RWN. The reason may be multifactorial. First, when designing the RNI, a certain smoothing treatment was performed after the segmentation (see Section 2.2), as the rough surface of the segmented model is not conducive to 3D printing. Consequently, slight alterations in the dimensions of the RNI may have occurred as a result of this smoothing process. Secondly, it is important to acknowledge that the size of the RWN could be influenced by various factors, including but not limited to weight and sex, which should be investigated in the future. Moreover, as mentioned above, a one-size-fits-all model is designed to reduce the variability of animal experiments. The differences between guinea pigs are small but still exist, so it makes sense that a one-size-fits-all model cannot perfectly fit in all guinea pig RWN.

Due to the design of the handle, the RNI can be inserted easily and correctly. The histology showed that the surgery did not cause any damage to other structures. A question that needs to be addressed in future is whether the RNI may have an impact on the traveling sound wave. The stapes of the middle ear asserts pressure on the oval window. This pressure from the stapes causes a movement in the scala tympani perilymph. This fluid pressure wave causes a traveling wave moving down the length of the basilar membrane onto the round window. If the RNI hinders the traveling sound wave moving the RWM, the hearing threshold may be affected. The key point is that the implant should well attach to the RWM but should not affect the RWM movement at the same time. Future studies have to reveal the impact of the RNI on the hearing threshold.

Since the intended function of the RNI is local drug delivery, the drug mixing and release are critical. We tested DEX as a model drug. DEX is widely used in clinic and preclinical trials. The DEX was easily mixed with the non-crosslinked silicone using a speedmixer™ and the imaging proved a homogeneous distribution in the printed RNI. The RNI with up to 20% DEX is biocompatible and effectively reduces TNFα production *in vitro*. Considering the bio-efficacy and cost, 1% DEX-RNI is nontoxic while exhibiting high activity and seen as an optimal DEX-loaded RNI candidate for future studies. This is why the 1% DEX GP-RNI was chosen for the release studies presented here. The *in vitro* drug release test of 1% DEX-RNI revealed detectable and sustained release of DEX throughout the entire 29-day experimental duration, albeit with a burst release within the first 24 h. Subsequently, the release rate attenuated. The measurable total amount of drug within the implant, the drug release rate over time, the cumulative drug release amount and sustained release duration constitute crucial parameters that serve as vital references for subsequent *in vivo* investigations. These findings enhance the controllability and predictability of RNI based local drug application. However, it must be kept in mind that different conditions prevail in the *in vitro* test compared to the expected situation *in vivo* where the implant is placed in the RWN and drug is expected to diffuse through the RWM in order to gain access to the site of action. For the sake of the analysis, a release volume was chosen for the *in vitro* study, which does not reflect the physiological volumes at the site of application. In addition, the release took place in a release medium that has been adapted to the analytical method and does not correspond to the composition of fluids at the site of application. Furthermore, no tissue simulation was performed during the release study and *in vivo* only parts of the surface of the implant are in direct contact with tissue. Sink conditions were maintained during the release study, in spite of the small media volumes used.

In the study presented here, the 1%, 5%, 10% and 20% DEX loaded samples all caused a comparable anti-inflammatory effect *in vitro*. Providing 1% DEX GP-RNI in cochlear implanted guinea pigs reduced the fibrosis around the CI electrode significantly compared to animals not receiving a GP-RNI. This suggests that the DEX diffused through the RWM into the perilymph where its anti-inflammatory action reduced the electrode insertion trauma induced immune response. If higher drug load will result in increased biological effects *in vivo*, i.e., reduced fibrosis or residual hearing preservation compared to 1% DEX loaded RNI has to be investigated in future studies. In the used animal model a cochleostomy with subsequent CI insertion was performed. While it cannot be ruled out that the DEX diffusing from the RNI has entered the inner ear via the cochleostomy as well, this assumption

is rather negligible because: I. various animal studies have shown that DEX diffuses very well through the RWM, II. the cochleostomy is located approximately 2 mm away from the niche and is sealed by the CI. If there is still a small gap between the CI and the bony cochlear wall, it is negligible compared to the contact surface between the RNI and the RWM, III: the DEX diffusion needs a concentration gradient between the RNI and the target structure. This is given between the RNI and the RWM by a small liquid film. Even though the middle ear cavity cannot be described as a dry environment, the bony cochlea wall between the RNI and the cochleostomy does not provide such a connection which may enable a concentration gradient.

1% DEX GP-RNI did not yield protective effects on residual hearing after the CI surgery. This observation prompts consideration of several contributing factors to residual hearing damage, including mechanical trauma, inflammation, shock waves in perilymph fluid, acoustic trauma due to drilling, loss of perilymph and bacterial infection (Von Ilberg et al., 2011). While DEX is recognized for its potential in preserving residual hearing, especially in high-frequency (James et al., 2008), repeated electrode insertions may induce severe and irreversible mechanical damage, resulting in DEX alone being insufficient in preserving residual hearing. Additionally, we speculate that the quantity of DEX penetrating the RWM may be inadequately low. Prior animal studies involving DEX administration via the RWM predominantly employed short-term (30 min to 120 min) applications, often in combination with gelatin or similar materials before surgery (James et al., 2008; Lee et al., 2013), making it challenging to determine the concentration that effectively permeates into the inner ear. Consequently, no definitive guinea pig data regarding the optimal DEX concentration for protecting residual hearing following cochlear implantation exist. The situation is even more difficult in patients. There it is nearly impossible to sample inner ear fluid for drug concentration analysis without causing tremendous damage to the hearing organ. Even though there is a variety of clinical trials investigating the effect of intratympanically applied steroids on hearing loss (Plontke et al., 2022) there is, to our knowledge, only one study reporting DEX concentrations in the inner ear after intratympanic application (Zhuo et al., 2023) and no data exist stating the concentration needed for hearing protection. Consequently, future studies have to elucidate which drug load is needed in the GP-RNI to achieve the optimal bioavailability at the target side. Finally, it is worth noting that the utility of RNI may hold additional advantages for CI patients in the long term. One approach could be the RNI implantation in patients' receiving a CI via cochleostomy. Studies have demonstrated the potential effectiveness of DEX in preventing delayed or progressive hearing loss, which can manifest days to months post-implantation. This phenomenon is hypothesized to be attributable to metabolic factors, encompassing inflammation, oxidative stress, and apoptosis (O'leary et al., 2013; Quesnel et al., 2016). In this case, RNI, designed for sustained drug release, emerge as a promising approach for the prevention and treatment of such conditions. A second approach could be the RNI implantation prior to CI implantation to modulate the cochlear environmental health. Application of the DEX loaded RNI several weeks prior to the opening of the cochlea may prepare the environment for the later CI-surgery, including the opening of the cochlea, and protect inner ear cells by preventing the activation of any damaging cascades in course of the surgery.

Based on the designed mean model for guinea pigs, the printing of the DEX containing silicone obtained an adequate GP-RNI for intratympanic drug delivery. Our study reports, for the first time, that a RNI can be built by 3D-printing of drug laden silicone, releases the drug, is biocompatible and has biological effects *in vitro* and *in vivo*. Future studies have to address the optimization of DEX load. Additionally, it is imperative to broaden the scope of clinical applications by exploring the potential of alternative and additional drugs. For instance, the local administration of gentamicin has demonstrated effectiveness in treating vestibular symptoms associated with Meniere's disease, while posing limited risks to hearing (Lange, 1989). To address pathologies such as Meniere's disease, tinnitus, noise, drug or age induced hearing loss, the RNI may be used to deliver multiple other active ingredients such as other steroids like prednisolone or triamcinolone through the intact RWM into the inner ear. It may be used to deliver e.g. cytostatics, proteins, peptides or gene vectors and potentially even cells, to enable local and sustained drug delivery when the matrix material is changed. Future studies need to investigate which ingredients can be incorporated, printed and released, as well as determining the appropriate preload concentrations and release rates needed to effectively treat patients. Additionally, approaches supporting the drug diffusion such as drug encapsulation into nanocarriers to improve RWM diffusion or RWM manipulation by e.g. enzymes to enhance drug entry into the inner ear should be addressed as well. In parallel with drug exploration, it is crucial to further investigate and evaluate various materials suitable for 3D printing. Currently, numerous bioprinting materials are undergoing investigation for potential clinical applications. The selection of appropriate printing materials should align with the pharmaceutical dosage forms and treatment requirements. Powdered drugs, for instance, exhibit compatibility with a wide range of 3D printing materials, while liquid dosage forms may necessitate the utilization of hydrogels. Moreover, biodegradable materials can avoid the need for explantation secondary surgery, thereby enhancing patient convenience and reducing healthcare burdens. By considering different drugs and selecting appropriate materials, the versatility and effectiveness of the GP-RNI platform can be enhanced.

5. Conclusion

Establishing effective pharmacotherapies for inner ear disorders is crucial. Using additive manufacturing, we developed a biocompatible RNI, which can be used for precise RWM drug delivery in guinea pigs as an animal model for inner ear disorders. The GP-RNI is precisely printable, the model drug DEX is homogenously distributed in the printed silicone, the GP-RNI extracts are biocompatible and bio-effective *in vitro*, the GP-RNI achieved a sustained drug release for more than 4 weeks and it is implantable in the RWN. The RNI containing 1% DEX has the anti-inflammatory potential concerning

fibrosis inhibition, but its beneficial effects on hearing preservation have yet to be demonstrated.

The initial findings of GP-RNI indicate promising results, suggesting progress in local drug delivery to the inner ear. This implant is engineered to achieve controlled and sustained release of pharmaceutical agents, potentially optimizing therapeutic effectiveness through improved pharmacokinetics and pharmacodynamics. Additionally, the technology underlying GP-RNI, namely 3D printing of drug-containing silicone, holds promise for advancing the management of inner ear disorders. Its capability to deliver multiple compounds concurrently may offer new possibilities for combination therapies, which could positively affect clinical outcomes. Moreover, GP-RNI serves as a prototype, providing valuable insights into the development of similar implants for various animal models and potentially for human patients. Through personalized and targeted delivery of therapeutic agents, this approach has the potential to contribute to enhancing the quality of life for individuals with inner ear disorders.

Acknowledgments

The authors thank MED-EL (Innsbruck, Austria) for providing the cochlear implants.

Ethical approval

All experiments were conducted in accordance with the German Animal Welfare Law and the European Directive 2010/63. In this study, all animals were Dunkin Hartley guinea pigs, including live ($N=14$) and cadavers ($N=23$). This investigation focused on the development of a drug-eluting implant manufactured by 3D printing. The objective is to adjust the implant's geometry to individual patient requirements and design the type and characteristics of the active ingredient load based on personalized considerations. The efficacy of RNI has shown promising clinical application potential in *in vitro* tests, however, further validation through *in vivo* tests are required. As an established cochlear pharmacology studies animal model, guinea pig is the most appropriate animal model to investigate the efficacy of this novel drug-eluting implant.

The DICOM data sets used to set up the GP-RNI design were generated as part of previous studies ($N=12$ cadavers from Charles River Laboratories, France) which were conducted with permission of the local authority (Lower Saxony State Office for Consumer Protection and Food Safety (LAVES), Oldenburg, Germany, registration number 19/3145 and 20/3502). The implantability tests, imaging and grinding were established on $N=11$ fresh cadavers (Dunkin-Hartley guinea pig) kindly provided by the working group of Prof. Mazzouli-Weber (Department of Physiology, University of Veterinary Medicine Hannover, Foundation, Hannover, Germany) for free. Those guinea pigs were killed by bolt shot in combination with throat transection, as permitted by the local authorities (§4) and we collected the heads immediately after the animals were dead, placed them on ice and stored them in −18 °C freezer until the experiments were performed.

The *in vivo* study on chronically implanted guinea pigs ($N=14$, Charles River Laboratories, France) was conducted with the explicit permission of the LAVES, registration number 20/3592). All experimental manipulations were performed under general anesthesia with intramuscular medetomidinhydrochloride (0.2 mg/kg), midazolam (1 mg/kg) and fentanyl (0.025 mg/kg). The anesthetized animals were always positioned on a 38 °C heating mat. The animals were allowed to acclimate to the animal facility for two weeks prior to treatment and were housed within a meticulously controlled environment, characterized by regulated temperature and humidity levels. A consistent 24-h light-dark cycle (14 h light, 10 h dark) was maintained to ensure a standardized living condition. Throughout the study, animals had unrestricted access to food and water to ensure their well-being and many efforts were undertaken to minimize their resultant distress. The authors have adhered to the ARRIVE guidelines.

Authors' contributions

Chunjiang Wei: conceptualization, investigation, methodology, formal analysis, validation, data curation, Writing – original draft and Writing – review and editing. Ziwen Gao: conceptualization, investigation, methodology, validation, writing – review and editing. Martina Knabel, Martin Ulbricht, Stefan Senekowitsch, Peter Erfurt, Norman Maggi and Bastian Zwick: methodology, formal analysis, writing – review and editing. Thomas Eickner, Farnaz Matin-Mann and Anne Seidlitz: methodology, writing – review and editing. Thomas Lenarz: resources, supervision, writing – review and editing. Verena Scheper: conceptualization, methodology, formal analysis, data curation, resources, project administration and Writing – review and editing. All authors read and approved the final version of the manuscript.

Disclosure statement

No potential conflict of interest was reported by the author(s).

Funding

This study was funded by the Federal Ministry of Education and Research of Germany (BMBF), 'RESPONSE – Partnership for Innovation in Implant Technology' in the program 'Zwanzig20 – Partnership for Innovation', Project ID [03ZZ0928L]. The first author is funded by the China Scholarship Council (CSC) from the Ministry of Education of P.R. China. This publication is funded by the Deutsche Forschungsgemeinschaft (DFG) as part of the 'Open Access Publikationskosten' program.

ORCID

Verena Scheper http://orcid.org/0000-0001-8618-8793

Data availability statement

The raw data supporting the conclusions of this article will be made available by the authors upon request.

References

Ahmadi N, Gausterer JC, Honeder C, et al. (2019). Long-term effects and potential limits of intratympanic dexamethasone-loaded hydrogels combined with dexamethasone-eluting cochlear electrodes in a low-insertion trauma Guinea pig model. Hear Res 384:107825. doi: 10.1016/j.heares.2019.107825.

Albuquerque AAS, Rossato M, Oliveira JAAd, Hyppolito MA. (2009). Understanding the anatomy of ears from guinea pigs and rats and its use in basic otologic research. Braz J Otorhinolaryngol 75:43–9.

Behrends W, Wulf K, Raggl S, et al. (2023). Dual drug delivery in cochlear implants: in vivo study of dexamethasone combined with diclofenac or immunophilin inhibitor MM284 in Guinea pigs. Pharmaceutics 15:726. doi: 10.3390/pharmaceutics15030726.

Bielefeld EC, Kopke RD, Jackson RL, et al. (2007). Noise protection with N-acetyl-l-cysteine (NAC) using a variety of noise exposures, NAC doses, and routes of administration. Acta Otolaryngol 127:914–9. doi: 10.1080/00016480601110188.

Bijarnia RK, Bachtler M, Chandak PG, et al. (2015). Sodium thiosulfate ameliorates oxidative stress and preserves renal function in hyperoxaluric rats. PLoS One 10:e0124881. doi: 10.1371/journal.pone.0124881.

Cederroth C, Gachon F, Canlon B. (2020). Time to listen: circadian impact on auditory research. Curr Opin Physiol 18:95–9. doi: 10.1016/j.cophys.2020.09.005.

Chang A, Eastwood H, Sly D, et al. (2009). Factors influencing the efficacy of round window dexamethasone protection of residual hearing post-cochlear implant surgery. Hear Res 255:67–72. doi: 10.1016/j.heares.2009.05.010.

Choe WT, Chinosornvatana N, Chang KW. (2004). Prevention of cisplatin ototoxicity using transtympanic N-acetylcysteine and lactate. Otol Neurotol 25:910–5. doi: 10.1097/00129492-200411000-00009.

Coleman JKM, Littlesunday C, Jackson R, Meyer T. (2007). AM-111 protects against permanent hearing loss from impulse noise trauma. Hear Res 226:70–8. doi: 10.1016/j.heares.2006.05.006.

Conlin AE, Parnes LS. (2007). Treatment of sudden sensorineural hearing loss: I. A systematic review. Arch Otolaryngol Head Neck Surg 133:573–81. doi: 10.1001/archotol.133.6.573.

Dodson KM, Woodson E, Sismanis A. (2004). Intratympanic steroid perfusion for the treatment of Meniere's disease: a retrospective study. Ear Nose Throat J 83:394–8. doi: 10.1177/014556130408300611.

Doyle KJ, Bauch C, Battista R, et al. (2004). Intratympanic steroid treatment: a review. Otol Neurotol 25:1034–9. doi: 10.1097/00129492-200411000-00031.

Ernfors P, Duan ML, ElShamy WM, Canlon B. (1996). Protection of auditory neurons from aminoglycoside toxicity by neurotrophin-3. Nat Med 2:463–7. doi: 10.1038/nm0496-463.

Fisher MJ, Lange BJ, Needle MN, et al. (2004). Amifostine for children with medulloblastoma treated with cisplatin-based chemotherapy. Pediatr Blood Cancer 43:780–4. doi: 10.1002/pbc.20132.

Förster CY, Shityakov S, Scheper V, Lenarz T. (2022). Linking cerebrovascular dysfunction to age-related hearing loss and Alzheimer's disease—are systemic approaches for diagnosis and therapy required? Biomolecules 12:1717. doi: 10.3390/biom12111717.

Gan RZ, Nakmali D, Zhang X. (2013). Dynamic properties of round window membrane in guinea pig otitis media model measured with electromagnetic stimulation. Hear Res 301:125–36. doi: 10.1016/j.heares.2013.01.001.

Gao Z, Schwieger J, Matin-Mann F, et al. (2021). Dexamethasone for inner ear therapy: Biocompatibility and bio-efficacy of different dexamethasone formulations in vitro. Biomolecules 11:1896. doi: 10.3390/biom11121896.

Gillespie LN, Clark GM, Bartlett PF, Marzella PL. (2003). BDNF-induced survival of auditory neurons in vivo: cessation of treatment leads to accelerated loss of survival effects. J Neurosci Res 71:785–90. doi: 10.1002/jnr.10542.

Gurney JG, Bass JK, Onar-Thomas A, et al. (2014). Evaluation of amifostine for protection against cisplatin-induced serious hearing loss in children treated for average-risk or high-risk medulloblastoma. Neuro Oncol 16:848–55. doi: 10.1093/neuonc/not241.

Hauser E. (1959). Ménière's disease: a new therapeutic approach. J Am Geriatr Soc 7:874–76.

Heffner HE, Heffner RS. (2007). Hearing ranges of laboratory animals. J Am Assoc Lab Anim Sci 46:20–2.

International Organization for Standardization. (2021). ISO 10993-12:2021(En). Biological evaluation of medical devices—part 12: Sample preparation and reference materials. Geneva: ISO.

James DP, Eastwood H, Richardson RT, O'Leary SJ. (2008). Effects of round window dexamethasone on residual hearing in a Guinea pig model of cochlear implantation. Audiol Neurootol 13:86–96. doi: 10.1159/000111780.

Kanzaki S, Stöver T, Kawamoto K, et al. (2002). Glial cell line-derived neurotrophic factor and chronic electrical stimulation prevent VIII cranial nerve degeneration following denervation. J Comp Neurol 454:350–60. doi: 10.1002/cne.10480.

Lange G. (1989). Gentamicin and other ototoxic antibiotics for the transtympanic treatment of Meniere's disease. Arch Otorhinolaryngol 246:269–70. doi: 10.1007/BF00463571.

Lee J, Ismail H, Lee JH, et al. (2013). Effect of both local and systemically administered dexamethasone on long-term hearing and tissue response in a Guinea pig model of cochlear implantation. Audiol Neurootol 18:392–405. doi: 10.1159/000353582.

Lexow GJ, Schurzig D, Gellrich N-C, et al. (2016). Visualization, measurement and modelling of the cochlea using rotating midmodiolar slice planes. Int J Comput Assist Radiol Surg 11:1855–69. doi: 10.1007/s11548-016-1374-7.

Malfeld K, Armbrecht N, Pich A, et al. (2022). Prevention of noise-induced hearing loss in vivo: continuous application of insulin-like growth factor 1 and its effect on inner ear synapses, auditory function and perilymph proteins. Int J Mol Sci 24:291. doi: 10.3390/ijms24010291.

Malfeld K, Baumhoff P, Volk HA, et al. (2022). Local long-term inner ear drug delivery in normal hearing guinea pig—an animal model to develop preventive treatment for noise-induced hearing loss. Biomolecules 12:1427. doi: 10.3390/biom12101427.

Matin F, Gao Z, Repp F, et al. (2021). Determination of the round window niche anatomy using cone beam computed tomography imaging as preparatory work for individualized drug-releasing implants. J Imaging 7:79. doi: 10.3390/jimaging7050079.

Matin-Mann F, Gao Z, Schwieger J, et al. (2022). Individualized, additively manufactured drug-releasing external ear canal implant for prevention of postoperative restenosis: development, in vitro testing, and proof of concept in an individual curative trial. Pharmaceutics 14:1242. doi: 10.3390/pharmaceutics14061242.

Mau R, Eickner T, Jüttner G, et al. (2023). Micro injection molding of drug-loaded round window niche implants for an animal model using 3D-printed molds. Pharmaceutics 15:1584. doi: 10.3390/pharmaceutics15061584.

Naert G, Pasdelou M-P, Le Prell CG. (2019). Use of the guinea pig in studies on the development and prevention of acquired sensorineural hearing loss, with an emphasis on noise. J Acoust Soc Am 146:3743–69. doi: 10.1121/1.5132711.

O'leary S, Monksfield P, Kel G, et al. (2013). Relations between cochlear histopathology and hearing loss in experimental cochlear implantation. Hear Res 298:27–35. doi: 10.1016/j.heares.2013.01.012.

Peitersen E, Carlson BH. (1966). Hearing impairment as the initial sign of polyarteritis nodosa. Acta Otolaryngol 61:189–95. doi: 10.3109/00016486609127055.

Plontke SK, Meisner C, Agrawal S, et al. (2022). Intratympanic corticosteroids for sudden sensorineural hearing loss. Cochrane Database Syst Rev 7:CD008080. doi: 10.1002/14651858.CD008080.pub2.

Quesnel AM, Nakajima HH, Rosowski JJ, et al. (2016). Delayed loss of hearing after hearing preservation cochlear implantation: human temporal bone pathology and implications for etiology. Hear Res 333:225–34. doi: 10.1016/j.heares.2015.08.018.

Rushworth GF, Megson IL. (2014). Existing and potential therapeutic uses for N-acetylcysteine: the need for conversion to intracellular glutathione for antioxidant benefits. Pharmacol Ther 141:150–9. doi: 10.1016/j.pharmthera.2013.09.006.

Scheper V, Hoffmann A, Gepp MM, et al. (2019). Stem cell based drug delivery for protection of auditory neurons in a guinea pig model of cochlear implantation. Front Cell Neurosci 13:177. doi: 10.3389/fncel.2019.00177.

Schindler RA, Gladstone HB, Scott N, et al. (1995). Enhanced preservation of the auditory nerve following cochlear perfusion with nerve growth factors. Am J Otol 16:304–9.

Shah SB, Gladstone HB, Williams H, et al. (1995). An extended study: protective effects of nerve growth factor in neomycin-induced auditory neural degeneration. Am J Otol 16:310–4.

Shea JJ, Jr, Ge X. (1996). Dexamethasone perfusion of the labyrinth plus intravenous dexamethasone for Meniere's disease. Otolaryngol Clin North Am 29:353–8. doi: 10.1016/S0030-6665(20)30398-4.

Shea JJ. (1983). Autoimmune sensorineural hearing loss as an aggravating factor in Meniere's disease. In: Neurophysiological and clinical aspects of vestibular disorders. Basel, Switzerland: Karger Publishers, 254–7. doi: 10.1159/000407651.

Sieber D, Erfurt P, John S, et al. (2019). The OpenEar library of 3D models of the human temporal bone based on computed tomography and micro-slicing. Sci Data 6:180297. doi: 10.1038/sdata.2018.297.

Silverstein H, Isaacson JE, Olds MJ, et al. (1998). Dexamethasone inner ear perfusion for the treatment of Meniere's disease: a prospective, randomized, double-blind, crossover trial. Otol Neurotol 19:196–201.

Smith JL. (1970). Cogan's syndrome. Laryngoscope 80:121–32. doi: 10.1288/00005537-197001000-00010.

Staecker H, Gabaizadeh R, Federoff H, Water TRVD. (1998). Brain-derived neurotrophic factor gene therapy prevents spiral ganglion degeneration after hair cell loss. Otolaryngol Head Neck Surg 119:7–13. doi: 10.1016/S0194-5998(98)70194-9.

Staecker H, Kopke R, Malgrange B, et al. (1996). NT-3 and/or BDNF therapy prevents loss of auditory neurons following loss of hair cells. Neuroreport 7:889–94. doi: 10.1097/00001756-199603220-00011.

Stebbins W, Moody D, Serafin J. (1982). Some principal issues in the analysis of noise effects on hearing in experimental animals. Am J Otolaryngol 3:295–304. doi: 10.1016/s0196-0709(82)80069-0.

Stephens SD, Luxon L, Hinchcliffe R. (1982). Immunological disorders and auditory lesions. Audiology 21:128–48. doi: 10.3109/00206098209072734.

Von Ilberg CA, Baumann U, Kiefer J, et al. (2011). Electric-acoustic stimulation of the auditory system: a review of the first decade. Audiol Neurootol 16:1–30. doi: 10.1159/000327765.

Wang Y, Qu Y, Chen X, et al. (2019). Effects of D-methionine in mice with noise-induced hearing loss mice. J Int Med Res 47:3874–85. doi: 10.1177/0300060519860679.

Watanabe H, Kysar JW, Lalwani AK. (2014). Microanatomic analysis of the round window membrane by white light interferometry and micro-computed tomography for mechanical amplification. Otol Neurotol 35:672–8. doi: 10.1097/MAO.0000000000000193.

Wever EG, Vernon JA, Peterson EA. (1963). The high-frequency sensitivity of the guinea pig ear. Proc Natl Acad Sci U S A 49:319–22. doi: 10.1073/pnas.49.3.319.

Wilk M, Hessler R, Mugridge K, et al. (2016). Impedance changes and fibrous tissue growth after cochlear implantation are correlated and can be reduced using a dexamethasone eluting electrode. PLoS One 11:e0147552. doi: 10.1371/journal.pone.0147552.

World Health Organization. (2014). Making fair choices on the path to universal health coverage: final report of the WHO consultative group on equity and universal health coverage. Geneva: World Health Organization.

Yagi M, Kanzaki S, Kawamoto K, et al. (2000). Spiral ganglion neurons are protected from degeneration by GDNF gene therapy. J Assoc Res Otolaryngol 1:315–25. doi: 10.1007/s101620010011.

Ylikoski J, Pirvola U, Virkkala J, et al. (1998). Guinea pig auditory neurons are protected by glial cell line-derived growth factor from degeneration after noise trauma. Hear Res 124:17–26. doi: 10.1016/s0378-5955(98)00095-1.

Zhuo S, Li Y, Cui B, et al. (2023). Round window niche veil is visible on high-resolution computed tomography and a predictor of local drug efficacy to inner ear. Laryngoscope 134:1396–402. doi: 10.1002/lary.31006.